Olutayo *et al. EURASIP Journal on Wireless Communications and Networking* (2020) 2020:97
https://doi.org/10.1186/s13638-020-01705-5

EURASIP Journal on Wireless Communications and Networking

RESEARCH Open Access

Performance bounds for diversity receptions over a new fading model with arbitrary branch correlation

Adebola Olutayo*, Julian Cheng and Jonathan F. Holzman

*Correspondence:
adebola.olutayo@alumni.ubc.ca
School of Engineering, The University of British Columbia, Kelowna, British Columbia, Canada

Abstract

The performance of a new (Beaulieu-Xie) fading model is analyzed using bounds. This recently proposed fading model can be used to describe both line-of-sight and non-line-of-sight components of a fading channel having different diversity orders. We consider the outage probability and error rate performance of maximal ratio combining, equal-gain combining, and selection combining over arbitrarily correlated Beaulieu-Xie fading channels. Closed-form expressions for upper and lower bounds to the outage probability and error rate are obtained, and it is shown that these bounds are asymptotically tight in the high signal-to-noise ratio regime. The analytical results are verified via Monte Carlo simulations. It is shown that the Beaulieu-Xie fading model can be more useful than the Ricean and Nakagami-*m* fading models in characterizing environments with both line-of-sight and multiple reflected specular components.

Keywords: 6G, Bounds, Correlation, Diversity, Fading channels, Outage probability, Level crossing rate, mmWave, Random access channels, THz

1 Introduction

Numerous models have been developed to characterize wireless communication systems. The Ricean fading model has been largely employed to characterize wireless systems with the presence of both a line-of-sight (LOS) signal and multi-path (non-LOS) signals. However, the Ricean fading model has a disadvantage in terms of its inadaptability to fading variations in the environment and its restriction to a diversity order of one [1]. The Nakagami-*m* fading model, which can be derived from the central chi-distribution, was proposed to characterize wireless systems over different fading variations. This is enabled by its flexible fading parameter *m*. It has been shown that the Nakagami-*m* fading model is practical when characterizing systems with multi-path signals. However, it is only suitable for systems with multi-path (non-LOS) signals [2–4].

A new fading model [1], which we and others refer to as the Beaulieu-Xie (BX) fading model [6–9], was recently proposed to overcome the limitations of both the Ricean and Nakagami-*m* fading models. This model, derived from the non-central chi-distribution in an identical manner in which the central chi-distribution was transformed to the Nakagami-*m* fading model, has a fading parameter *m*, LOS power λ^2, and non-LOS power

Ω. More importantly, it has the ability to characterize wireless systems with multiple LOS and non-LOS components. The normalization that leads to the BX fading model is carried out by scaling the random variable (RV), R, which is distributed according to non-central chi distribution by a factor $\sqrt{\frac{2m}{\Omega}}$ to have another RV, Z which is distributed according to the BX distribution, such that $R = Z\sqrt{\frac{2m}{\Omega}}$. In doing this, the non-centrality parameter λ in the non-central chi distribution is also scaled by the factor $\sqrt{\frac{2m}{\Omega}}$ so that its relationship with the parameter λ in the BX distribution, which for clarity we refer to as λ^*, becomes $\lambda = \lambda^*\sqrt{\frac{2m}{\Omega}}$ [1]. This normalization process ensures that the effect of the anomaly of unbounded fading power found in the non-central chi-distribution is eliminated. It is important to comment that the $\kappa - \mu$ (or generalized Ricean) distribution, unlike the BX fading model, does not have a proper normalization. In fact, the BX fading model is a normalized form of the $\kappa - \mu$ (or generalized Ricean) model [1], as will be shown in Section 3. This leads to the $\kappa - \mu$ model having an unbounded fading power just as it is found in the non-central chi-distribution. This major flaw is evident in its second moment (also known as the instantaneous power) which is dependent on the degrees of freedom. Hence, the $\kappa - \mu$ (or generalized Ricean) distribution violates the principle of physical fading channels and should not be used to describe a fading environment.

The flexibility presented by the BX fading model, by way of its three parameters, makes it of interest in representations of practical fading for future femtocell, millimeter-wave (mmWave), and terahertz (THz) communication systems, as well as 6G short-range random access channels, where multiple components are present due to signal reflections [1]. In addition, the BX fading model exhibits a seamless relationship to other fading models, such as the Ricean, Nakagami-m, and Rayleigh fading models. The relationship between the BX, Ricean, Nakagami-m, and Rayleigh distribution is feasible because these four fading models all have bounded fading powers which is evident in their second moment. In the absence of LOS components, the BX fading model becomes the Nakagami-m fading model just as the Ricean fading model becomes the Rayleigh fading model. Also, when the fading parameter m is equal to 1, the BX fading model becomes the Ricean fading model just as the Nakagami-m fading model becomes the Rayleigh fading model.

The merits of the BX fading model and its improved ability to characterize channels for emerging wireless communication systems can be demonstrated using the experimental data obtained from cross-polarized LOS measurements of 28-GHz outdoor mmWave channels published in [5]. It can be shown via the goodness-of-fit of the fading models, quantified by the Kolmogorov-Smirnov (KS) test, that the BX fading model shows an improved fit in comparison to the fit for the Ricean fading model. Despite its theoretical and practical importance, to the best of the authors' knowledge, there has been no performance analysis of wireless systems on BX channels reported beyond the works in [6–11].

Although the performance of correlated $\kappa - \mu$ (or generalized Ricean) fading channels [12] have been analyzed in [13], it is not meaningful to study arbitrary correlation of such a fading model as it does not satisfy the power constraint. This is evident in its parameter κ (and the K-factor in the generalized Ricean model) in that changes in the degrees of freedom, according to the severity of fading, must be compensated for by adjusting the non-LOS parameter. This is done to keep the total power of the scattering component

invariant [1]. In contrast, adjusting the fading parameter, m, in BX fading does not affect the power in the scatter component [1].

Given the merits of the BX fading model for future femtocell, mmWave, and THz communication systems, as well as 6G short-range random access channels, it is important to recognize the assumption of independent fading in implementing spatial diversity. Such an assumption requires that there be sufficient spacing between the channels and this may often not be the case [14]. A separation of 30 to 50 wavelengths between channels is typically required to obtain correlation coefficients between 0 and 0.33 [15, 16]. With this in mind, we consider the effects of correlation in this work for BX fading channels with maximal ratio combining (MRC), equal-gain combining (EGC), and selective combining (SC). The analysis targets performance bounds to evaluate the performance—in recognition of the fact that intractable integrals/infinite series arise in the pursuit of closed-form expressions. A recently developed bounding technique [17] is applied here. The key idea of this bounding technique is to handle correlated fading amplitude involving BX RVs by transforming the original problem into a new problem involving correlated Gaussian RVs, whose joint probability density function (pdf) can lead to tractable upper and lower bounds of the joint pdf near the origin. This technique enables two main contributions. First, asymptotically tight error rate and outage probability (OP) bounds (at high SNR) are derived in closed-form for diversity receptions over arbitrarily correlated BX channels. These tight bounds are obtained by bounding the pdf of the associated nonzero-mean Gaussian RVs. Second, we show that the diversity receptions over arbitrarily correlated BX fading channels outperform those of Nakagami-m fading channels, given that this latter model lacks the ability to characterize LOS components. Ultimately, the analytical results are verified by Monte Carlo simulations and are compared to those in literature.

The remainder of the paper is organized as follows. In Section 2, we summarize the analytical methods of this work. In Section 3, we discuss the physicality (and justification) of the BX fading model. In Section 4, we introduce the system model for linear diversity receptions in BX fading. We discuss the merits of the BX fading model and the employed bound analysis. In Section 5, we show the relationship between the power correlation and Gaussian correlation coefficient, and in Section 6, we derive bounds on the pdf of the channel coefficient. In Sections 8 and 9, we analyze and discuss the asymptotically tight bounds on the OP and error rate for MRC, SC, and EGC schemes. Section 10 presents numerical results, and Section 11 gives some concluding remarks.

2 Method

This paper analyses performance bounds on the OP and error rate for diversity reception over arbitrarily correlated BX fading. The work considers MRC, EGC, and SC techniques, with expressions for the upper and lowers bound in closed form. The closed-form expressions are obtained by transforming the original problem involving correlated fading amplitude RVs to a new problem involving correlated Guassian RVs, whose joint pdf leads to amenable bounds close to the origin. The results obtained analytically are confirmed by Monte Carlo simulations in MATLAB with different parameters and are compared to those in literature. The effect of correlation on system performance is also illustrated.

3 Physicality and justification of the BX fading model

The performance analyses put forward in this work are motivated by the BX fading

model's ability to characterize wireless systems with multiple LOS and non-LOS components while satisfying the physical constraint of power conservation. It will be shown in this section that the BX fading model's ability to handle this power constraint comes about from its normalization—and this sets it apart from the existing $\kappa - \mu$ fading model and the equivalent generalized Ricean fading model. We consider here various distributions for the fading models. For the $\kappa - \mu$ fading model, the pdf is defined for a RV of G by

$$f_G(g) = \frac{2\mu\,(1+\kappa)^{\frac{\mu+1}{2}}}{\hat{g}\kappa^{\frac{\mu-1}{2}}\exp(\mu\kappa)}\left(\frac{g}{\hat{g}}\right)^{\mu} \times \exp\left[-\mu\,(1+\kappa)\left(\frac{g}{\hat{g}}\right)^{2}\right] I_{\mu-1}\left[2\mu\sqrt{\kappa\,(1+\kappa)}\frac{g}{\hat{g}}\right] \tag{1}$$

where μ is the positive-valued fading parameter, $\hat{g}$ is the square-root of the second moment defined as $\hat{g} = \sqrt{E\left[G^2\right]}$, and κ is the ratio of total power for the LOS and non-LOS components. With such definitions, d sets the total power for the LOS components at d^2 and σ sets the total power for the non-LOS components at $2n\sigma^2$, given n as the number of Gaussian RVs [12]. For the generalized Ricean fading model, the pdf is defined for a RV of F by transforming (1) with substitutions of s^2 for d^2, n for μ, and $\sqrt{2n\sigma^2 + s^2}$ for $\hat{d}$. This gives a pdf of

$$f_F(f) = \frac{f^{\frac{n}{2}}}{\sigma^2 s^{\frac{n-2}{2}}}\exp\left(-\frac{f^2+s^2}{2\sigma^2}\right) \times I_{\frac{n}{2}-1}\left(\frac{fs}{\sigma^2}\right) \tag{2}$$

where s sets the total power for the LOS components at s^2. With such definitions, $K = s^2/2n\sigma^2$ is the K-factor and $E\left[F^2\right] = 2n\sigma^2 + s^2$ is the second-order moment. Ultimately, the above definitions for κ, K, and $E\left[F^2\right]$ all depend upon n, and this leads to two shortcomings for the $\kappa - \mu$ and generalized Ricean distributions: (i) the power of the non-LOS components has to be adjusted to keep the total power invariant and (ii) the fading powers of both distributions are unbounded. Nonetheless, these shortcomings can be overcome by normalization—and this is done by the BX fading model. The BX RV, Z, can be obtained by normalizing the generalized Ricean distribution in (2) such that $F = Z\sigma\sqrt{2m/\Omega}$ and $s = \lambda\sigma\sqrt{2m/\Omega}$. This produces a pdf for the BX fading model in the form of

$$f_Z(z) = \frac{\exp\left(-\frac{m}{\Omega}\left(z^2+\lambda^2\right)\right) z^m \left(\frac{2m}{\Omega}\right)}{\lambda^{m-1}} I_{m-1}\left(\frac{2m}{\Omega}\lambda z\right) \tag{3}$$

where m is the fading parameter. With such definitions, $K = \lambda^2/\Omega$ is the K-factor given λ^2 as the LOS power and Ω as the non-LOS power. For this pdf of the BX fading model, m controls the shape, Ω controls the spread, and λ impacts the location and height of the mode [1, 6].

The physicality and manifestation of the BX fading model can be seen by the fact that its distribution becomes an impulse at $\sqrt{\lambda^2 + \Omega}$ as the fading parameter, m, approaches infinity just like the Nakagami-m distribution tends to an impulse at $\sqrt{\Omega}$. To see this, we define the generalized Ricean RV as

$$F = \sqrt{\sum_{i=1}^{n} V_i^2} \tag{4}$$

where V_i is a Gaussian distributed RV with mean m_i and variance σ^2 and n is the number of Gaussian RVs. We obtain the BX RV, Z, via normalization such that

$$Z = \frac{\sqrt{\sum_{i=1}^{n} V_i^2}}{\sigma\sqrt{\frac{n}{\Omega}}} = \frac{\sqrt{\Omega}}{\sigma}\sqrt{\frac{\sum_{i=1}^{n} V_i^2}{n}} \tag{5}$$

while noting that $n = 2m$. When m and thus n approach infinity, we are left with the BX RV's limit of

$$Z_{\text{lim}} = \lim_{n\to\infty} \frac{\sqrt{\Omega}}{\sigma}\sqrt{\frac{\sum_{i=1}^{n} V_i^2}{n}}. \tag{6}$$

This limit can be simplified using the Chebyshev's law of large numbers [18] to

$$\lim_{n\to\infty}\sqrt{\frac{\sum_{i=1}^{n} V_i^2}{n}} = \lim_{n\to\infty}\sqrt{\frac{1}{n}\sum_{i=1}^{n} E\left[V_i^2\right]}. \tag{7}$$

We note here that s in (2) is defined as $s = \sqrt{\sum_{i=1}^{n} m_i^2}$, which allows (7) to be cast as

$$\lim_{n\to\infty}\sqrt{\sigma^2 + \frac{s^2}{n}}. \tag{8}$$

We also note that the parameter λ in (3) is scaled by $\sigma\sqrt{\frac{2m}{\Omega}}$, which gives $\lambda = \frac{s}{\sigma\sqrt{\frac{2m}{\Omega}}}$. Applying this scaling to (8) and inserting the result into (6) gives

$$Z_{\text{lim}} = \lim_{n\to\infty} \frac{\sqrt{\Omega}}{\sigma}\sqrt{\sigma^2 + \frac{\sigma^2\lambda^2}{n}} = \sqrt{\lambda^2 + \Omega}. \tag{9}$$

We see from this last expression that the limiting RV of Z_{lim} is a constant at $\sqrt{\lambda^2 + \Omega}$. Thus, the distribution of Z takes the form of an impulse at $z = \sqrt{\lambda^2 + \Omega}$ as m approaches infinity—which cannot be said of the $\kappa - \mu$ or generalized Ricean distributions. Moreover, the location of the impulse for the BX distribution, like the Nakagami-m distribution, corresponds to the square-root of the second-order moment (or instantaneous power) of its distribution and this quantity is bounded.

4 System model

We consider linear diversity receptions with N branches operating over the channels described by the BX fading model. The received signal is

$$\mathbf{y} = \mathbf{z}x + \mathbf{n} \tag{10}$$

where x is the transmitted signal, $\mathbf{n}$ is a random vector denoting additive Gaussian white noise (AWGN), and $\mathbf{z}$ is the fading channel vector, i.e., the real fading channel amplitudes. In addition, $\mathbf{z} = [z_1, \ldots, z_N]^T = \left[\sqrt{\bar{\gamma}_1}Z_1, \ldots, \sqrt{\bar{\gamma}_N}Z_N\right]^T$, where $[\cdot]^T$ represents the transpose, $\bar{\gamma}_n$ is the average received SNR of the nth branch, Z_n is the fading amplitude of the nth branch, and z is distributed according to (3).

The respective output SNRs for MRC, EGC, and SC diversity receptions are

$$\gamma_{\text{MRC}} = \sum_{n=1}^{N} \bar{\gamma}_n Z_n^2 \tag{11a}$$

$$\gamma_{\text{EGC}} = \frac{1}{N}\left(\sum_{n=1}^{N} \sqrt{\bar{\gamma}_n} Z_n\right)^2 \tag{11b}$$

$$\gamma_{\text{SC}} = \max\left(\bar{\gamma}_1 Z_1^2, \cdots, \bar{\gamma}_n Z_n^2\right). \tag{11c}$$

We assume that the BX RV is associated with the nth branch as

$$Z_n = \sqrt{\sum_{i=1}^{2m} X_{n,i}^2};\ \ \forall n = 1, \ldots N \tag{12}$$

where $X_{n,i}$, $\forall i = 1, \ldots 2m$ are Gaussian RVs with mean μ and variance $\left(\frac{1}{2m}\right)$. Here, m is a half-integer representing the fading parameter that controls the shape of the pdf in the fading model. The nth component of $\mathbf{z}$ can be obtained by generating an $N \times 2m$ matrix of Gaussian RVs, $\mathbf{B}$, whose entries are $b_{n,i}$ and whose mth column is denoted as $\mathbf{b}_m$, such that $\mathbf{B} = [\mathbf{b}_1, \ldots, \mathbf{b}_{2m}]$. We obtain the vector $\mathbf{b} = \left[\mathbf{b}_1^T, \ldots, \mathbf{b}_{2m}^T\right]^T = \left[b_{1,1}, b_{2,1}, \ldots, b_{n,2m}\right]^T$. We can, therefore, express the fading amplitude over the nth branch as

$$z_n = \sqrt{\sum_{i=1}^{2m} b_{n,i}^2};\ \ \forall n = 1, \ldots N \tag{13}$$

such that $b_{n,i}^2 = \bar{\gamma}_n X_{n,i}^2$.

The pdf of $\mathbf{b}$ is expressed as

$$f_{\mathbf{b}}(\mathbf{b}) = \frac{1}{\sqrt{(2\pi)^{2mN}\,|\mathbf{R_b}|}} \times \exp\left(-\frac{1}{2}\left(\mathbf{b} - \boldsymbol{\mu}_{\mathbf{b}}\right)^T \mathbf{R}_{\mathbf{b}}^{-1}\left(\mathbf{b} - \boldsymbol{\mu}_{\mathbf{b}}\right)\right) \tag{14}$$

where $\boldsymbol{\mu}_{\mathbf{b}}$ is the $2mN \times 1$ mean vector and $\mathbf{R_b}$ is the $2mN \times 2mN$ covariance matrix of $\mathbf{b}$. The variances of the LOS and non-LOS components are defined as $\sigma_{L,n}^2 = \left|\mu_{b,n}\right|^2$ and $\sigma_{NL,n}^2 = E\left[\left|b_n - \mu_{b,n}\right|^2\right]$, respectively, where $|\cdot|$ denotes magnitude and $E[\cdot]$ denotes expectation. The K-factor for the BX fading channel is therefore defined as $K = \frac{\sigma_{L,n}^2}{\sigma_{NL,n}^2}$. The determinant of the covariance matrix $\mathbf{R_b}$ is expressed in terms of the correlation matrix $\mathbf{C_b}$ by $|\mathbf{R_b}| = \frac{\left(\prod_{n=1}^{N} \bar{\gamma}_n^{2m}\right)|\mathbf{C_b}|}{(2m)^{2mN}}$ [17]. This new fading model has the diversity order mN which is the same as that of the Nakagami-m fading model, for the same value of m, but the former predicts improved performance for channels possessing LOS components [1].

5 Relationship between the power correlation and Gaussian correlation coefficient

As shown in [16], the correlation coefficient between RVs $X_{n,i}$ and $X_{j,k}$ with mean μ and variance $\frac{1}{2m}$ is obtained by employing the Cholesky decomposition. It can be shown that $X_{n,i} = \rho_{(n,i)(j,k)} X_{j,k} + \sqrt{1 - \rho_{(n,i)(j,k)}^2}\, W$, where $\rho_{(n,i)(j,k)}$ is the correlation coefficient and W is a Gaussian RV with zero mean and variance $\frac{1}{2m}$, which is independent of $X_{j,k}$. This

leads to a relationship between the power correlation coefficient, $\rho_{z_{n_1}^2 z_{n_2}^2}$, and correlation coefficient of the Gaussian RVs, $\rho_{(n,i)(j,k)}$, according to

$$\rho_{z_{n_1}^2 z_{n_2}^2} = \frac{D - (2m)^2 T^2}{(2+2m)\, U - (2m)^2 T^2} \tag{15}$$

where

$$D = \sum_{i=1}^{2m} \sum_{k=1}^{2m} \left(3U^2 \rho_{(n,i)(j,k)}^2 + T^2 \left(1 - \rho_{(n,i)(j,k)}^2 \right) \right),$$

$T = \frac{1}{2m} + \mu^2$, and $U = \frac{1}{2m}$. A special case can be obtained when $\mu = 0$ such that

$$\rho_{z_{n_1}^2 z_{n_2}^2} = \frac{1}{2m} \sum_{i=1}^{2m} \sum_{k=1}^{2m} \rho_{(n,i)(j,k)}^2 \tag{16}$$

which is the same as the one obtained for the Nakagami-m fading model in [17], as expected.

6 Bounds to the pdf

Here, we show that the pdf of $\mathbf{b}$ is bounded in the region $\mathbf{b}^T\mathbf{b} \leq r^2$, which is a $2mN$-dimensional sphere with radius r. A Rayleigh quotient is applied, such that $R_y\left(\mathbf{R}_\mathbf{b}^{-1}, \mathbf{b}\right) = \frac{\mathbf{b}^T \mathbf{R}_\mathbf{b}^{-1} \mathbf{b}}{\mathbf{b}^T \mathbf{b}}$, where $\mathbf{R_b}$ is a positive definite matrix. The numerical range of R_y is obtained as $\lambda_{\min} \leq \frac{\mathbf{b}^T \mathbf{R}_\mathbf{b}^{-1} \mathbf{b}}{\mathbf{b}^T \mathbf{b}} \leq \lambda_{\max}$, such that λ_i are the eigenvalues of $\mathbf{R}_\mathbf{b}^{-1}$ and $\lambda_i \geq 0$, where [19] $\lambda_{\min}$ is the smallest eigenvalue of $\mathbf{R}_\mathbf{b}^{-1}$, and $\lambda_{\max}$ is the largest eigenvalue of $\mathbf{R}_\mathbf{b}^{-1}$. Thus, considering the region $\mathbf{b}^T\mathbf{b} \leq r^2$, we take $\lambda_{\min} = 0$ to give

$$0 \leq \mathbf{b}^T \mathbf{R}_\mathbf{b}^{-1} \mathbf{b} \leq \lambda_{\max} \mathbf{b}^T \mathbf{b}. \tag{17}$$

We expand the exponential component with the knowledge that ${\mathbf{R}_\mathbf{b}^{-1}}^T = \mathbf{R}_\mathbf{b}^{-1}$; this gives

$$(\mathbf{b} - \boldsymbol{\mu_b})^T \mathbf{R}_\mathbf{b}^{-1} (\mathbf{b} - \boldsymbol{\mu_b}) = \mathbf{b}^T \mathbf{R}_\mathbf{b}^{-1} \mathbf{b} + \boldsymbol{\mu_b}^T \mathbf{R}_\mathbf{b}^{-1} \boldsymbol{\mu_b} + 2 \left| \boldsymbol{\mu_b}^T \mathbf{R}_\mathbf{b}^{-1} \mathbf{b} \right|. \tag{18}$$

We employ the 2-norm of the matrix as $\|\mathbf{b}\| = \sqrt{\mathbf{b^T b}} = r$, such that (18) becomes

$$\begin{aligned} &- 2 \left\| \boldsymbol{\mu_b}^T \mathbf{R}_\mathbf{b}^{-1} \right\| r + \boldsymbol{\mu_b}^T \mathbf{R}_\mathbf{b}^{-1} {\boldsymbol{\mu_b}}^T \\ &\leq \left(\mathbf{b} - \boldsymbol{\mu_b} \right)^T \mathbf{R}_\mathbf{b}^{-1} \left(\mathbf{b} - \boldsymbol{\mu_b} \right) \\ &\leq \lambda_{\max} r^2 + 2 \left\| \boldsymbol{\mu_b}^T \mathbf{R}_\mathbf{b}^{-1} \right\| r + \boldsymbol{\mu_b}^T \mathbf{R}_\mathbf{b}^{-1} {\boldsymbol{\mu_b}}^T. \end{aligned} \tag{19}$$

The upper and lower bounds of $f_\mathbf{b}(\mathbf{b})$ near the origin are then obtained as

$$\begin{aligned} &f_\mathbf{b}(\mathbf{0}) \exp\left(-\frac{1}{2} \left(\lambda_{\max} r^2 + 2 \left\| \boldsymbol{\mu_b}^T \mathbf{R}_\mathbf{b}^{-1} \right\| r \right) \right) \\ &\leq f_\mathbf{b}(\mathbf{b}) \leq f_\mathbf{b}(\mathbf{0}) \exp\left(\left\| \boldsymbol{\mu_b}^T \mathbf{R}_\mathbf{b}^{-1} \right\| r \right). \end{aligned} \tag{20}$$

7 Performance bounds to outage probability

The OP and error rate of diversity combining schemes are two important performance metrics that can be used to quantify the effects of correlated fading. We analyze the performance of this new fading model here with arbitrary channel correlation by computing the bounds according to [17]. Here, we set an SNR threshold, γ_{th}, below which we declare occurrences of outage.

7.1 Outage probability bounds for MRC

We express the OP for MRC with respect to a signal threshold, γ_{th}, as

$$P_o^{\text{MRC}}(\gamma_{th}) = \Pr\{\gamma_{\text{MRC}} \leq \gamma_{\text{th}}\}. \tag{21}$$

Substituting (12) into (11a) and then substituting the result into (21) leads to

$$\begin{aligned} P_o^{\text{MRC}}(\gamma_{th}) &= \Pr\left\{\sum_{n=1}^{N}\sum_{i=1}^{2m} b_{n,i}^2 \leq \gamma_{\text{th}}\right\} \\ &= \int\limits_{\gamma_{\text{MRC}} \leq \gamma_{\text{th}}} f_{\mathbf{b}}(\mathbf{b}) d\mathbf{b}. \end{aligned} \tag{22}$$

It should be noted that the above integral is a $2mN$-fold integral, but for notational simplicity, it is expressed with just one integral sign.

7.1.1 Asymptotic outage probability approximation for MRC

The asymptotic OP approximation is obtained by substituting $f_{\mathbf{b}}(\mathbf{b}) \approx f_{\mathbf{b}}(\mathbf{0})$ into (22), where

$$f_{\mathbf{b}}(\mathbf{0}) = \frac{1}{\sqrt{(2\pi)^{2\,\text{mN}}\,|\mathbf{R}_{\mathbf{b}}|}} \exp\left(-\frac{1}{2}\boldsymbol{\mu}^T \mathbf{R}_{\mathbf{b}}^{-1} \boldsymbol{\mu}_{\mathbf{b}}\right)$$

and simplifying to give

$$P_{o,\infty}^{\text{MRC}}(\gamma_{\text{th}}) = f_{\mathbf{b}}(\mathbf{0}) \int\limits_{\gamma_{\text{MRC}} \leq \gamma_{\text{th}}} d\mathbf{b} \tag{23}$$

where $\gamma_{\text{MRC}} = \sum\limits_{n=1}^{N}\sum\limits_{i=1}^{2m} b_{n,i}^2$. The integral in (23) is the volume of a $2mN$ dimensional sphere with a radius of $r = \sqrt{\gamma_{\text{th}}}$. Ultimately, Eq. (23) can be expressed as

$$P_{o,\infty}^{\text{MRC}}(\gamma_{\text{th}}) = f_{\mathbf{b}}(\mathbf{0}) \frac{\left(2\sqrt{\gamma_{th}}\right)^{2\,\text{mN}+1} \pi^{\text{mN}} \Gamma(\text{mN}+1)}{(2\,\text{mN}+1)!}. \tag{24}$$

7.1.2 Lower bound outage probability for MRC

The lower bound to the OP is obtained by replacing $f_{\mathbf{b}}(\mathbf{0})$ with the lower bound of the pdf obtained in (20) into (23). Substituting the result into (23) gives

$$P_{o,\text{LM}}^{\text{MRC}}(\gamma_{\text{th}}) = O_{LM} \int\limits_{\gamma_{\text{MRC}} \leq \gamma_{\text{th}}} d\mathbf{b} \tag{25}$$

where

$$O_{\text{LM}} = f_{\mathbf{b}} \times (\mathbf{0}) \exp\left(-\frac{1}{2}\left(\lambda_{\max}\gamma_{\text{th}} + 2\left\|\boldsymbol{\mu}_{\mathbf{b}}{}^T \mathbf{R}_{\mathbf{b}}^{-1}\right\| \sqrt{\gamma_{\text{th}}}\right)\right).$$

Eq. 25 can be further simplified to

$$P_{o,\text{LB}}^{\text{MRC}}(\gamma_{\text{th}}) = O_{\text{LM}} \times \left[\frac{\left(2\sqrt{\gamma_{\text{th}}}\right)^{(2\text{mN}+1)} \pi^{\text{mN}} \Gamma(\text{mN}+1)}{(2\text{mN}+1)!}\right]. \tag{26}$$

7.1.3 Upper bound outage probability for MRC

The upper bound to the OP is obtained by replacing $f_{\mathbf{b}}(\mathbf{0})$ with the upper bound of the pdf obtained in (20) and by substituting the result into (23). This gives

$$P_{o,UB}^{\text{MRC}}(\gamma_{\text{th}}) = O_{\text{UM}} \int\limits_{\gamma_{\text{MRC}} \leq \gamma_{\text{th}}} d\mathbf{b} \tag{27}$$

where $O_{\mathrm{UM}} = f_{\mathbf{b}}(\mathbf{0}) \exp\left(\left\|\boldsymbol{\mu}_{\mathbf{b}}{}^{T}\mathbf{R}_{\mathbf{b}}^{-1}\right\| \sqrt{\gamma_{\mathrm{th}}}\right)$. Eq. 27 is further simplified to

$$P_{o,LB}^{\mathrm{MRC}}(\gamma_{\mathrm{th}}) = O_{\mathrm{UM}} \times \left[\frac{\left(2\sqrt{\gamma_{\mathrm{th}}}\right)^{(2\,\mathrm{mN}+1)} \pi^{\mathrm{mN}} \Gamma(\mathrm{mN}+1)}{(2\,\mathrm{mN}+1)!}\right]. \tag{28}$$

We compare the results obtained in (24), (26), and (28), observing that $O_{LM} \leq f_{\mathbf{b}}(\mathbf{b}) \leq O_{\mathrm{UM}}$, which is the same as (20). It is seen that the difference between the bounds lies in the exponential component of the equations. An increase to the average SNR per branch leads to the lower and upper bounds of the OP converging to the asymptotic approximation.

7.2 Outage probability bounds for EGC

We express the OP for EGC with respect to a signal threshold, γ_{th}, as

$$P_o^{\mathrm{EGC}}(\gamma_{\mathrm{th}}) = \Pr\{\gamma_{\mathrm{EGC}} \leq \gamma_{\mathrm{th}}\}. \tag{29}$$

Substituting (12) into (11b) and then substituting the result into (29) gives

$$\begin{aligned} P_o^{\mathrm{EGC}}(\gamma_{\mathrm{th}}) &= \Pr\left\{\frac{1}{N}\left(\sum_{n=1}^{N}\sqrt{\sum_{i=1}^{2m} b_{n,i}^2}\right)^2 \leq \gamma_{\mathrm{th}}\right\} \\ &= \int_{\gamma_{\mathrm{EGC}} \leq \gamma_{\mathrm{th}}} f_{\mathbf{b}}(\mathbf{b}) d\mathbf{b}. \end{aligned} \tag{30}$$

7.2.1 Asymptotic outage probability approximation for EGC

The asymptotic OP approximation is obtained by substituting $f_{\mathbf{b}}(\mathbf{b}) \approx f_{\mathbf{b}}(\mathbf{0})$ in (30) and simplifying to give

$$P_{o,\infty}^{\mathrm{EGC}}(\gamma_{\mathrm{th}}) = f_{\mathbf{b}}(\mathbf{0}) \int_{\gamma_{\mathrm{EGC}} \leq \gamma_{\mathrm{th}}} d\mathbf{b} \tag{31}$$

where $\gamma_{\mathrm{EGC}} = \frac{1}{N}\left(\sum_{n=1}^{N}\sqrt{\sum_{i=1}^{2m} b_{n,i}^2}\right)^2$. The integral in (31) is obtained as [17]

$$\int_{\gamma_{\mathrm{EGC}} \leq \gamma_{\mathrm{th}}} d\mathbf{b} = \left(\frac{2m\pi^m}{\Gamma(m+1)}\right)^N \frac{\Gamma^N(2m)}{(2mN)} (N\gamma_{\mathrm{th}})^{\mathrm{mN}}. \tag{32}$$

This result in (32) is substituted into (31) to give the asymptotic OP approximation as

$$P_{o,\infty}^{\mathrm{EGC}}(\gamma_{\mathrm{th}}) = f_{\mathbf{b}}(\mathbf{0}) \left(\frac{2m\pi^m}{\Gamma(m+1)}\right)^N \frac{\Gamma^N(2m)}{(2\,\mathrm{mN})} (N\gamma_{\mathrm{th}})^{\mathrm{mN}}. \tag{33}$$

7.2.2 Lower bound outage probability for EGC

We compare the integral region for EGC to that of MRC. These integral regions can be expressed as

$$IR_{\mathrm{EGC}}(r) \triangleq \left\{\frac{1}{N}\sum_{n=1}^{N}\sum_{i=1}^{2m} b_{n,i}^2 \leq r^2\right\}$$

and

$$\mathrm{IR}_{\mathrm{MRC}}(r) \triangleq \left\{\sum_{n=1}^{N}\sum_{i=1}^{2m} b_{n,i}^2 \leq r^2\right\}.$$

Note that $\sum_{n=1}^{N}\sum_{i=1}^{2m} b_{n,i}^2 \leq Nr^2$ can be derived from $\frac{1}{N}\sum_{n=1}^{N}\sum_{i=1}^{2m} b_{n,i}^2 \leq r^2$. Thus, the integral region $\mathrm{IR}_{\mathrm{EGC}}(r)$ lies within $\mathrm{IR}_{\mathrm{MRC}}\left(\sqrt{N}r\right)$. We then obtain a bound on the pdf for EGC by substituting r with $\sqrt{N}r$ in (20) as

$$f_{\mathbf{b}}(\mathbf{0}) \exp\left(-\frac{1}{2}\left(\lambda_{\max} N r^2 + 2\left\|\boldsymbol{\mu}_{\mathbf{b}}{}^T \mathbf{R}_{\mathbf{b}}^{-1}\right\| \sqrt{N}r\right)\right) \leq f_{\mathbf{b}}(\mathbf{b}) \leq f_{\mathbf{b}}(\mathbf{0}) \exp\left(\left\|\boldsymbol{\mu}_{\mathbf{b}}{}^T \mathbf{R}_{\mathbf{b}}^{-1}\right\| \sqrt{N}r\right) \tag{34}$$

where $r = \sqrt{\gamma_{\mathrm{th}}}$. Substituting the lower bound of the result obtained in (34) into (31), the lower bound OP for EGC is obtained as

$$P_{o,\mathrm{LB}}^{\mathrm{EGC}}(\gamma_{\mathrm{th}}) = O_{\mathrm{LE}} \times \int_{\gamma_{\mathrm{EGC}} \leq \gamma_{\mathrm{th}}} d\mathbf{b} \tag{35}$$

where

$$O_{\mathrm{LE}} = f_{\mathbf{b}}(\mathbf{0}) \times \exp\left(-\frac{1}{2}\left(\lambda_{\max} N \gamma_{\mathrm{th}} + 2\left\|\boldsymbol{\mu}_{\mathbf{b}}{}^T \mathbf{R}_{\mathbf{b}}^{-1}\right\| \sqrt{N\gamma_{th}}\right)\right).$$

This result can be expressed as

$$P_{o,\mathrm{LB}}^{\mathrm{EGC}}(\gamma_{\mathrm{th}}) = O_{\mathrm{LE}} \times \left(\frac{2m\pi^m}{\Gamma(m+1)}\right)^N \frac{\Gamma^N(2m)}{(2\,\mathrm{mN})} (N\gamma_{\mathrm{th}})^{\mathrm{mN}}. \tag{36}$$

7.2.3 Upper bound outage probability for EGC

The upper bound to the OP of EGC is obtained by replacing $f_{\mathbf{b}}(\mathbf{0})$ in (31) by the upper bound of the pdf in (34), which gives

$$P_{o,\mathrm{UB}}^{\mathrm{EGC}}(\gamma_{\mathrm{th}}) = O_{\mathrm{UE}} \times \int_{\gamma_{\mathrm{EGC}} \leq \gamma_{\mathrm{th}}} d\mathbf{b} \tag{37}$$

where $O_{\mathrm{UE}} = f_{\mathbf{b}}(\mathbf{0}) \exp\left(\left\|\boldsymbol{\mu}_{\mathbf{b}}{}^T \mathbf{R}_{\mathbf{b}}^{-1}\right\| \sqrt{N\gamma_{\mathrm{th}}}\right)$. This result can be expressed as

$$P_{o,\mathrm{UB}}^{\mathrm{EGC}}(\gamma_{\mathrm{th}}) = O_{\mathrm{UE}} \times \left(\frac{2m\pi^m}{\Gamma(m+1)}\right)^N \frac{\Gamma^N(2m)}{(2\,\mathrm{mN})} (N\gamma_{\mathrm{th}})^{\mathrm{mN}}. \tag{38}$$

We compare the results obtained in (33), (36), and (38), observing that $O_{\mathrm{LE}} \leq f_{\mathbf{b}}(\mathbf{b}) \leq O_{\mathrm{UE}}$ is the same as (34). It is seen again that the difference between the bounds lies in the exponential components of the equations. An increase to the average SNR per branch leads to the lower and upper bounds of the OP converging to the asymptotic approximation, as was found previously.

7.3 Outage probability bounds for SC

We express the OP for SC with respect to a signal threshold, γ_{th}, as

$$P_o^{\mathrm{SC}}(\gamma_{\mathrm{th}}) = \Pr\{\gamma_{\mathrm{SC}} \leq \gamma_{\mathrm{th}}\}. \tag{39}$$

Substituting (12) into (11c) gives

$$P_o^{\mathrm{SC}}(\gamma_{\mathrm{th}}) = \Pr\left\{\max_n \left\{\sum_{i=1}^{2m} b_{n,i}^2\right\} \leq \gamma_{\mathrm{th}}\right\} = \int_{\gamma_{\mathrm{SC}} \leq \gamma_{\mathrm{th}}} f_{\mathbf{b}}(\mathbf{b}) d\mathbf{b}. \tag{40}$$

7.3.1 Asymptotic outage probability approximation for SC

The asymptotic OP approximation is obtained by substituting $f_{\mathbf{b}}(\mathbf{b}) \approx f_{\mathbf{b}}(\mathbf{0})$ into (40) and simplifying to give

$$P_{o,\infty}^{\mathrm{SC}}(\gamma_{\mathrm{th}}) = f_{\mathbf{b}}(\mathbf{0}) \prod_{n=1}^{N} \int_{\sum_{i=1}^{2m} b_{n,i}^2 \le \gamma_{\mathrm{th}}} d\mathbf{b}_n \tag{41}$$

where $d\mathbf{b}_n = \Pi_{n=1}^{N} db_{n,i}$. The integral in (41) is the $2m$-dimensional volume of a ball with a radius of $r = \sqrt{\gamma_{\mathrm{th}}}$. Ultimately, Eq. (41) can be expressed as

$$P_{o,\infty}^{\mathrm{SC}}(\gamma_{\mathrm{th}}) = f_{\mathbf{b}}(\mathbf{0}) \times \left[\frac{\left(2\sqrt{\gamma_{\mathrm{th}}}\right)^{(2m+1)} \pi^m \Gamma(m+1)}{(2m+1)!} \right]^N. \tag{42}$$

7.3.2 Lower bound outage probability for SC

We compare the integral region for SC to that of MRC. These integral regions can be expressed as

$$\mathrm{IR}_{\mathrm{SC}}(r) \triangleq \left\{ \max_n \left\{ \sum_{i=1}^{2m} b_{n,i}^2 \right\} \le r^2 \right\}$$

and

$$\mathrm{IR}_{\mathrm{MRC}}(r) \triangleq \left\{ \sum_{n=1}^{N} \sum_{i=1}^{2m} b_{n,i}^2 \le r^2 \right\}$$

where r is the radius. We can therefore bound the $2m$-dimensional ball in (41) by the hypersphere in (23). In addition, we note that $\sum_{n=1}^{N} \sum_{i=1}^{2m} b_{n,i}^2 \le Nr$ can be derived from $\max_n \left\{ \sum_{i=1}^{2m} b_{n,i}^2 \right\} \le r$; therefore, $\mathrm{IR}_{\mathrm{SC}}(r)$ lies within $\mathrm{IR}_{\mathrm{MRC}}\left(\sqrt{N}r\right)$. Equation 34 is therefore an applicable bound to SC. Substituting the lower bound of the result obtained in (34) into (41) gives

$$P_{o,\mathrm{LB}}^{\mathrm{SC}}(\gamma_{\mathrm{th}}) = O_{\mathrm{LS}} \int_{\gamma_{\mathrm{SC}} \le \gamma_{\mathrm{th}}} d\mathbf{b} \tag{43}$$

where

$$O_{\mathrm{LS}} = f_{\mathbf{b}}(\mathbf{0}) \times \exp\left(-\frac{1}{2} \left(\lambda_{\max} N \gamma_{\mathrm{th}} + 2 \left\| \boldsymbol{\mu}_{\mathbf{b}}{}^T \mathbf{R}_{\mathbf{b}}^{-1} \right\| \sqrt{N\gamma_{\mathrm{th}}} \right) \right).$$

Equation 43 can be further simplified to

$$P_{o,\mathrm{LB}}^{\mathrm{SC}}(\gamma_{\mathrm{th}}) = O_{\mathrm{LS}} \times \left[\frac{\left(2\sqrt{\gamma_{\mathrm{th}}}\right)^{(2m+1)} \pi^m \Gamma(m+1)}{(2m+1)!} \right]^N. \tag{44}$$

7.3.3 Upper bound outage probability for SC

The upper bound to the OP is obtained by replacing $f_{\mathbf{b}}(\mathbf{0})$ in (40) with the upper bound of the pdf obtained in (34). This gives

$$P_{o,\mathrm{UB}}^{\mathrm{SC}}(\gamma_{\mathrm{th}}) = O_{\mathrm{US}} \int_{\gamma_{\mathrm{SC}} \le \gamma_{\mathrm{th}}} d\mathbf{b} \tag{45}$$

where $O_{\mathrm{US}} = f_{\mathbf{b}}(\mathbf{0}) \exp\left(\left\|\boldsymbol{\mu}_{\mathbf{b}}{}^{T}\mathbf{R}_{\mathbf{b}}^{-1}\right\| \sqrt{N\gamma_{\mathrm{th}}}\right)$. Equation 45 is further simplified to

$$P_{o,\mathrm{UB}}^{\mathrm{SC}}(\gamma_{\mathrm{th}}) = O_{\mathrm{US}} \times \left[\frac{\left(2\sqrt{\gamma_{\mathrm{th}}}\right)^{(2m+1)} \pi^{m} \Gamma(m+1)}{(2m+1)!}\right]^{N}. \tag{46}$$

We compare the results obtained in (42), (44), and (46), observing that $O_{\mathrm{LS}} \leq f_{\mathbf{b}}(\mathbf{b}) \leq O_{\mathrm{US}}$ is the same as (34). It is once again seen that the difference between the bounds lies in the exponential components of the equations. An increase to the average SNR per branch leads to the lower and upper bounds of the OP converging to the asymptotic approximation, as seen previously.

8 Performance bounds to error rate

8.1 Error rate bounds for MRC

We can express the error rate for MRC as

$$\begin{aligned} P_{e}^{\mathrm{MRC}} &= E\left[pQ\left(\sqrt{q\sum_{n=1}^{N}\sum_{i=1}^{2m} b_{n,i}^{2}}\right)\right] \\ &= p\int_{-\infty}^{\infty} Q\left(\sqrt{q\sum_{n=1}^{N}\sum_{i=1}^{2m} b_{n,i}^{2}}\right) f_{\mathbf{b}}(\mathbf{b})\, d\mathbf{b} \end{aligned} \tag{47}$$

where the Gaussian Q-function is defined as [20, 21]

$$Q(x) = \frac{1}{\sqrt{2\pi}} \int_{x}^{\infty} \exp\left(\frac{-t^{2}}{x}\right) dt.$$

For the special case of coherent binary phase shift keying (BPSK), we have $p = 1$ and $q = 2$.

8.1.1 Asymptotic error rate approximation for MRC

The asymptotic error rate approximation is obtained by substituting $f_{\mathbf{b}}(\mathbf{b}) \approx f_{\mathbf{b}}(\mathbf{0})$ into (47) to give

$$P_{e,\infty}^{\mathrm{MRC}} = p f_{\mathbf{b}}(\mathbf{0}) \int_{-\infty}^{\infty} Q\left(\sqrt{q\sum_{n=1}^{N}\sum_{i=1}^{2m} b_{n,i}^{2}}\right) d\mathbf{b} \tag{48}$$

where the integral in (48) is obtained as [17, 22, 23]

$$\int_{-\infty}^{\infty} Q\left(\sqrt{q\sum_{n=1}^{N}\sum_{i=1}^{2m} b_{n,i}^{2}}\right) d\mathbf{b} = \frac{2^{\mathrm{mN}-1}\pi^{\mathrm{mN}}}{q^{\mathrm{mN}}\sqrt{\pi}} \frac{\Gamma\left(\mathrm{mN}+\frac{1}{2}\right)}{\Gamma(\mathrm{mN}+1)}. \tag{49}$$

Substituting (49) into (48) gives the asymptotic error rate bound as

$$P_{e,\infty}^{\mathrm{MRC}} = p f_{\mathbf{b}}(\mathbf{0}) \frac{2^{\mathrm{mN}-1}\pi^{\mathrm{mN}}}{q^{\mathrm{mN}}\sqrt{\pi}} \frac{\Gamma\left(\mathrm{mN}+\frac{1}{2}\right)}{\Gamma(\mathrm{mN}+1)}. \tag{50}$$

8.1.2 Lower error rate bound for MRC

The lower bound to the error rate is obtained by changing the integral region in (48) according to

$$P_e^{\mathrm{MRC}} = p \int\limits_{R_{\mathrm{MRC}} \le R_{\mathrm{th}}^2} Q\left(\sqrt{q \sum_{n=1}^{N} \sum_{i=1}^{2m} b_{n,i}^2}\right) \times f_{\mathbf{b}}(\mathbf{b})\, d\mathbf{b} \tag{51}$$

where $R_{\mathrm{MRC}} = \sum\limits_{n=1}^{N} \sum\limits_{i=1}^{2m} b_{n,i}^2$. Substituting $f_{\mathbf{b}}(\mathbf{b})$ with the lower bound of the pdf in (20) into (51), where $r = R_{\mathrm{th}}$, and applying some simplifications, we have

$$P_{e,LB}^{\mathrm{MRC}} = p \times E_{\mathrm{LM}} \times G(R_{\mathrm{th}}) \tag{52}$$

where

$$E_{\mathrm{LM}} = f_{\mathbf{b}}(\mathbf{0}) \times \exp\left(-\frac{1}{2}\left(\lambda_{\max} {R_{\mathrm{th}}}^2 + 2\left\|{\boldsymbol{\mu}_{\mathbf{b}}}^T \mathbf{R}_{\mathbf{b}}^{-1}\right\| R_{\mathrm{th}}\right)\right) \tag{53}$$

and

$$G(R_{\mathrm{th}}) = \frac{\pi^{\mathrm{mN}}}{\Gamma(\mathrm{mN}+1)}\left[{R_{\mathrm{th}}}^{2\,\mathrm{mN}} Q\left(\sqrt{q} R_{\mathrm{th}}\right) + \frac{2^{\mathrm{mN}-1}}{q^{\mathrm{mN}}\sqrt{\pi}} \gamma\left(\mathrm{mN}+\frac{1}{2}, \frac{q}{2}{R_{\mathrm{th}}}^2\right)\right] \tag{54}$$

where $\gamma(\alpha, x) = \int\limits_0^x e^{-t} t^{\alpha-1} dt$ is the incomplete gamma function [17, 24].

8.1.3 Upper error rate bound for MRC

We obtain the upper bound to the error rate by splitting the integral region in (48) according to

$$\begin{aligned} P_{e,\mathrm{UB}}^{\mathrm{MRC}} = p \times & \int\limits_{R_{\mathrm{MRC}} \le R_{\mathrm{th}}^2} f_{\mathbf{b}}(\mathbf{b})\, Q\left(\sqrt{q \sum_{n=1}^{N} \sum_{i=1}^{2m} b_{n,i}^2}\right) d\mathbf{b} \\ & + p \int\limits_{R_{\mathrm{MRC}} > R_{\mathrm{th}}^2} f_{\mathbf{b}}(\mathbf{b})\, Q\left(\sqrt{q \sum_{n=1}^{N} \sum_{i=1}^{2m} b_{n,i}^2}\right) d\mathbf{b}. \end{aligned} \tag{55}$$

We consider the upper bound of the pdf obtained in (20) such that (55) can be expressed as [25]

$$\begin{aligned} P_{e,\mathrm{UB}}^{\mathrm{MRC}} = p \times E_{\mathrm{UM}} \times & \int\limits_{R_{\mathrm{MRC}} \le R_{\mathrm{th}}^2} Q\left(\sqrt{q \sum_{n=1}^{N} \sum_{i=1}^{2m} b_{n,i}^2}\right) d\mathbf{b} \\ & + p f_{\mathbf{b}}\left(\boldsymbol{\mu}_{\mathbf{b}}\right) \int\limits_{R_{\mathrm{MRC}} > R_{\mathrm{th}}^2} Q\left(\sqrt{q \sum_{n=1}^{N} \sum_{i=1}^{2m} b_{n,i}^2}\right) d\mathbf{b} \end{aligned} \tag{56}$$

where the first integral in (56) can be simplified as in (54), $f_{\mathbf{b}}(\mathbf{b})$ is substituted with the upper bound in (20) where $E_{\mathrm{UM}} = f_{\mathbf{b}}(\mathbf{0}) \exp\left(\left\|{\boldsymbol{\mu}_{\mathbf{b}}}^T \mathbf{R}_{\mathbf{b}}^{-1}\right\| R_{\mathrm{th}}\right)$, and $f_{\mathbf{b}}(\mathbf{b})$ is substituted with $f_{\mathbf{b}}\left(\boldsymbol{\mu}_{\mathbf{b}}\right)$ obtained as

$$f_{\mathbf{b}}(\mathbf{b}) = \frac{1}{\sqrt{(2\pi)^{2\,\mathrm{mN}} |\mathbf{R}_{\mathbf{b}}|}},$$

which is the largest value of $f_{\mathbf{b}}(\mathbf{b})$ in the second part of (55). The second integral in (56) is obtained as

$$H(R_{\text{th}}) = \int_{R_{\text{SC}}>R_{\text{th}}^2} Q\left(\sqrt{q\sum_{n=1}^{N}\sum_{i=1}^{2m} b_{n,i}^2}\right) d\mathbf{b} \left\{ \frac{\pi^{\text{mN}} 2^{\text{mN}-1}\Gamma\left(\text{mN}+\frac{1}{2}\right)}{\Gamma(\text{mN}+1)\sqrt{\pi}q^{\text{mN}}} - \frac{\pi^{\text{mN}}}{\Gamma(\text{mN}+1)} \times \left[{R_{\text{th}}}^{2\text{mN}} Q\left(\sqrt{q}R_{\text{th}}\right) + \frac{2^{\text{mN}-1}}{\sqrt{\pi}q^{\text{mN}}}\gamma\left(\text{mN}+\frac{1}{2}, \frac{q}{2}R_{th}^2\right)\right]\right\}. \tag{57}$$

8.2 Error rate bounds for EGC

We can express the error rate for EGC as

$$P_e^{\text{EGC}} = E\left[pQ\left(\sqrt{\frac{q}{N}\left(\sum_{n=1}^{N}\sqrt{\sum_{i=1}^{2m} b_{n,i}^2}\right)^2}\right)\right] = p\int_{-\infty}^{\infty} Q\left(\sqrt{\frac{q}{N}\left(\sum_{n=1}^{N}\sqrt{\sum_{i=1}^{2m} b_{n,i}^2}\right)^2}\right) f_{\mathbf{b}}(\mathbf{b})\, d\mathbf{b}. \tag{58}$$

8.2.1 Asymptotic error rate approximation of EGC

The asymptotic error rate approximation is obtained by substituting $f_{\mathbf{b}}(\mathbf{b}) \approx f_{\mathbf{b}}(\mathbf{0})$ in (58) to give

$$P_{e,\infty}^{\text{EGC}} = p \times f_{\mathbf{b}}(\mathbf{0}) \times \int_{-\infty}^{\infty} Q\left(\sqrt{\frac{q}{N}\left(\sum_{n=1}^{N}\sqrt{\sum_{i=1}^{2m} b_{n,i}^2}\right)^2}\right) d\mathbf{b} \tag{59}$$

where we obtain the integral in (59) according to [11 Eq. (61)]. This is simplified to give

$$P_{e,\infty}^{\text{EGC}} = p f_{\mathbf{b}}(\mathbf{0}) \times Y(R_{\text{th}}) \tag{60}$$

where

$$Y(R_{\text{th}}) = \left(\frac{2m\pi^m}{\Gamma(m+1)}\right)^N \left(\frac{\Gamma^N(2m)}{\Gamma(2\text{mN})}\right) \times \left(\frac{N^{\text{mN}} 2^{\text{mN}-2}}{\sqrt{\pi}\,\text{mN} q^{\text{mN}}}\Gamma\left(\text{mN}+\frac{1}{2}\right)\right). \tag{61}$$

8.2.2 Lower Error Rate Bound for EGC

The lower bound to the error rate is obtained by changing the integral bound in (59) as

$$P_e^{\text{EGC}} = p \times \int_{R_{\text{EGC}}\le R_{\text{th}}^2} Q\left(\sqrt{\frac{q}{N}\left(\sum_{n=1}^{N}\sqrt{\sum_{i=1}^{2m} b_{n,i}^2}\right)^2}\right) \times f_{\mathbf{b}}(\mathbf{b})\, d\mathbf{b} \tag{62}$$

where $R_{\text{EGC}} = \sqrt{\frac{q}{N}\left(\sum_{n=1}^{N}\sqrt{\sum_{i=1}^{2m} b_{n,i}^2}\right)^2}$. Substituting $f_{\mathbf{b}}(\mathbf{b})$ with the lower bound of the pdf in (34) into (62), where $r = R_{\text{th}}$, and simplifying gives

$$P_{e,\text{LB}}^{\text{EGC}} = p f_{\mathbf{b}}(\mathbf{0}) \times E_{\text{LE}} \times W(R_{\text{th}}) \tag{63}$$

where

$$E_{\text{LE}} = f_{\mathbf{b}}(\mathbf{0}) \exp\left(-\frac{1}{2}\left(\lambda_{\max} N {R_{\text{th}}}^2 + 2\left\|\boldsymbol{\mu}_{\mathbf{b}}{}^T \mathbf{R}_{\mathbf{b}}^{-1}\right\|\sqrt{N}R_{\text{th}}\right)\right) \tag{64}$$

and

$$W\left(R_{\text{th}}\right)=\left(\frac{2m\pi^{m}}{\Gamma\left(m+1\right)}\right)^{N}\times\left(\frac{\Gamma^{N}\left(2m\right)}{\Gamma\left(2\,\text{mN}\right)}\right)\times\left[\left(\frac{2^{\text{mN}-2}N^{\text{mN}}}{\sqrt{\pi}\,\text{mN}q^{\text{mN}}}\;\gamma\left(\text{mN}+\frac{1}{2},\frac{q}{2}{R_{\text{th}}}^{2}\right)\right.\right.$$
$$\left.\left.+Q\left(\sqrt{q}R_{\text{th}}\right)\frac{{R_{th}}^{2\,\text{mN}}N^{\text{mN}}}{2\,\text{mN}}\right)\right]. \tag{65}$$

8.2.3 Upper error rate bound for EGC

The upper error rate bound is obtained by splitting the integral region in (58) according to

$$P_{e,UB}^{\text{EGC}}=p\int\limits_{R_{\text{EGC}}\leq R_{\text{th}}^{2}}Q\left(\sqrt{\frac{q}{N}\left(\sum_{n=1}^{N}\sqrt{\sum_{i=1}^{2m}b_{n,i}^{2}}\right)^{2}}\right)\times f_{\mathbf{b}}\left(\mathbf{b}\right)d\mathbf{b}$$
$$+p\int\limits_{R_{\text{EGC}}>R_{\text{th}}^{2}}Q\left(\sqrt{\frac{q}{N}\left(\sum_{n=1}^{N}\sqrt{\sum_{i=1}^{2m}b_{n,i}^{2}}\right)^{2}}\right)\times f_{\mathbf{b}}\left(\mathbf{b}\right)d\mathbf{b}. \tag{66}$$

We substitute $f_{\mathbf{b}}\left(\mathbf{b}\right)$ with the upper bound of the pdf in (20), for the first part, and $f_{\mathbf{b}}\left(\mathbf{b}\right)$ with $f_{\mathbf{b}}\left(\boldsymbol{\mu}_{\mathbf{b}}\right)$, which is the largest value of $f_{\mathbf{b}}\left(\mathbf{b}\right)$ for the second part. This gives

$$P_{e,UB}^{\text{EGC}}=p\times E_{\text{UE}}\times\int\limits_{R_{\text{EGC}}\leq R_{\text{th}}^{2}}Q\left(\sqrt{\frac{q}{N}\left(\sum_{n=1}^{N}\sqrt{\sum_{i=1}^{2m}b_{n,i}^{2}}\right)^{2}}\right)d\mathbf{b}$$
$$+pf_{\mathbf{b}}\left(\mu_{\mathbf{b}}\right)\times\underbrace{\int\limits_{R_{\text{EGC}}>{R_{\text{th}}}^{2}}Q\left(\sqrt{\frac{q}{N}\left(\sum_{n=1}^{N}\sqrt{\sum_{i=1}^{2m}b_{n,i}^{2}}\right)^{2}}\right)d\mathbf{b}}_{I\left(\boldsymbol{\mu}_{\mathbf{b}}\right)} \tag{67}$$

where $E_{\text{UE}}=f_{\mathbf{b}}\left(\mu_{\mathbf{b}}\right)\left(\mathbf{0}\right)\exp\left(\left\|\boldsymbol{\mu}_{\mathbf{b}}{}^{T}\mathbf{R}_{\mathbf{b}}^{-1}\right\|\sqrt{N}R_{\text{th}}\right)$. The first integral above is simplified as in (54), and the second integral is simplified as

$$I\left(\boldsymbol{\mu}_{\mathbf{b}}\right)=\int\limits_{-\infty}^{\infty}Q\left(\sqrt{\frac{q}{N}\left(\sum_{n=1}^{N}\sqrt{\sum_{i=1}^{2m}b_{n,i}^{2}}\right)^{2}}\right)d\mathbf{b}-\int\limits_{R_{\text{EGC}}\leq R_{\text{th}}^{2}}Q\left(\sqrt{\frac{q}{N}\left(\sum_{n=1}^{N}\sqrt{\sum_{i=1}^{2m}b_{n,i}^{2}}\right)^{2}}\right)d\mathbf{b}. \tag{68}$$

After some mathematical manipulation, Eq. (68) is further simplified to give

$$\int\limits_{R_{\text{EGC}}\leq R_{\text{th}}^{2}}Q\left(\sqrt{\frac{q}{N}\left(\sum_{n=1}^{N}\sqrt{\sum_{i=1}^{2m}b_{n,i}^{2}}\right)^{2}}\right)d\mathbf{b}\geq\int\limits_{R_{\text{EGC}}\leq R_{\text{th}}^{2}}Q\left(\sqrt{q\sum_{n=1}^{N}\sum_{i=1}^{2m}b_{n,i}^{2}}\right)d\mathbf{b}, \tag{69}$$

and then

$$=\int\limits_{-\infty}^{\infty}Q\left(\sqrt{\frac{q}{N}\left(\sum_{n=1}^{N}\sqrt{\sum_{i=1}^{2m}b_{n,i}^{2}}\right)^{2}}\right)d\mathbf{b}-\int\limits_{R_{\text{EGC}}\leq R_{\text{th}}^{2}}Q\left(\sqrt{q\sum_{n=1}^{N}\sum_{i=1}^{2m}b_{n,i}^{2}}\right)d\mathbf{b}. \tag{70}$$

Ultimately, Eq. (68) can be expressed as

$$Z(R_{\text{th}}) = Y(R_{\text{th}}) - \frac{\pi^{\text{mN}}}{\Gamma(\text{mN}+1)} \times \left[R_{\text{th}}^{2\text{mN}} Q\left(\sqrt{q} R_{\text{th}}\right) + \frac{2^{\text{mN}-1}}{\sqrt{\pi} q^{\text{mN}}} \gamma\left(\text{mN} + \frac{1}{2}, \frac{q}{2} R_{\text{th}}^2\right)\right]. \tag{71}$$

Substituting (65) and (71) into (67) gives the upper error rate bound for EGC.

8.3 Error rate bounds for SC

We can express the error rate for SC as

$$\begin{aligned} P_e^{\text{SC}} &= E\left[pQ\left(\sqrt{q \max_n \left\{ \sum_{i=1}^{2m} b_{n,i}^2 \right\}}\right)\right] \\ &= p \int_{-\infty}^{\infty} Q\left(\sqrt{q \max_n \left\{ \sum_{i=1}^{2m} b_{n,i}^2 \right\}}\right) f_{\mathbf{b}}(\mathbf{b})\, d\mathbf{b}. \end{aligned} \tag{72}$$

8.3.1 Asymptotic error rate approximation for SC

The asymptotic error rate approximation is obtained by substituting $f_{\mathbf{b}}(\mathbf{b}) \approx f_{\mathbf{b}}(\mathbf{0})$ into (72) to give

$$P_e^{\text{SC}} = p f_{\mathbf{b}}(\mathbf{0}) \int_{-\infty}^{\infty} Q\left(\sqrt{q \max_n \left\{ \sum_{i=1}^{2m} b_{n,i}^2 \right\}}\right) d\mathbf{b} \tag{73}$$

which can be simplified to [17, 26]

$$P_{e,\infty}^{\text{SC}} = p f_{\mathbf{b}}(\mathbf{0}) \frac{2^{\text{mN}-1} \pi^{\text{mN}} \Gamma\left(\text{mN} + \frac{1}{2}\right)}{q^{\text{mN}} \sqrt{\pi} \Gamma^N (m+1)}. \tag{74}$$

8.3.2 Lower error rate bound for SC

The lower bound of the error rate is obtained by changing the integral region in (72) according to

$$P_e^{\text{SC}} = p \int_{R_{\text{SC}} \le R_{\text{th}}^2} Q\left(\sqrt{q \max_n \left\{ \sum_{i=1}^{2m} b_{n,i}^2 \right\}}\right) \times f_{\mathbf{b}}(\mathbf{b})\, d\mathbf{b} \tag{75}$$

where $R_{\text{SC}} = \max_n \left\{ \sum_{i=1}^{2m} b_{n,i}^2 \right\}$. Substituting $f_{\mathbf{b}}(\mathbf{b})$ with the lower bound of the pdf in (34) into (75), where $r = R_{\text{th}}$, and simplifying gives

$$P_{e,\text{LB}}^{\text{SC}} = p \times E_{\text{LS}} \times S(R_{\text{th}}) \tag{76}$$

where

$$E_{\text{LS}} = f_{\mathbf{b}}(\mathbf{0}) \exp\left(-\frac{1}{2} \left(\lambda_{\max} N {R_{\text{th}}}^2 + 2 \left\| {\mu_{\mathbf{b}}}^T \mathbf{R}_{\mathbf{b}}^{-1} \right\| \sqrt{N} R_{\text{th}} \right) \right) \tag{77}$$

and

$$S(R_{\text{th}}) = \frac{\pi^{\text{mN}}}{\Gamma^N (m+1)} \left({R_{\text{th}}}^{2\text{mN}} Q\left(\sqrt{q} R_{\text{th}}\right) + \frac{2^{\text{mN}-1}}{q^{\text{mN}} \sqrt{\pi}} \gamma\left(\frac{2\text{mN}+1}{2}, \frac{q}{2} {R_{\text{th}}}^2 \right) \right). \tag{78}$$

8.3.3 Upper error rate bound for SC

The upper error rate bound is obtained by splitting the integral region in (72) according to

$$P_{e,\mathrm{UB}}^{\mathrm{SC}} = p \int\limits_{R_{\mathrm{SC}} \le R_{\mathrm{th}}^2} Q\left(\sqrt{q \max_n \left\{\sum_{i=1}^{2m} b_{n,i}^2\right\}}\right) f_{\mathbf{b}}(\mathbf{b})\, d\mathbf{b} + p \int\limits_{R_{\mathrm{SC}} > R_{\mathrm{th}}^2} Q\left(\sqrt{q \max_n \left\{\sum_{i=1}^{2m} b_{n,i}^2\right\}}\right) f_{\mathbf{b}}(\mathbf{b})\, d\mathbf{b}. \tag{79}$$

We consider the upper bound of the pdf obtained in (34) such that (79) can be expressed as

$$P_{e,UB}^{\mathrm{SC}} = p \times E_{\mathrm{UB}} \int\limits_{R_{\mathrm{SC}} \le R_{\mathrm{th}}^2} Q\left(\sqrt{q \max_n \left\{\sum_{i=1}^{2m} b_{n,i}^2\right\}}\right) d\mathbf{b} + p f_{\mathbf{b}}(\boldsymbol{\mu}_{\mathbf{b}}) \int\limits_{R_{\mathrm{SC}} > R_{\mathrm{th}}^2} Q\left(\sqrt{q \max_n \left\{\sum_{i=1}^{2m} b_{n,i}^2\right\}}\right) d\mathbf{b} \tag{80}$$

where the first integral is simplified as in (78) and $E_{\mathrm{UB}} = f_{\mathbf{b}}(\mathbf{0}) \exp\left(\left\|\boldsymbol{\mu}_{\mathbf{b}}{}^T \mathbf{R}_{\mathbf{b}}^{-1}\right\| \sqrt{N} R_{\mathrm{th}}\right)$. The second integral is obtained as

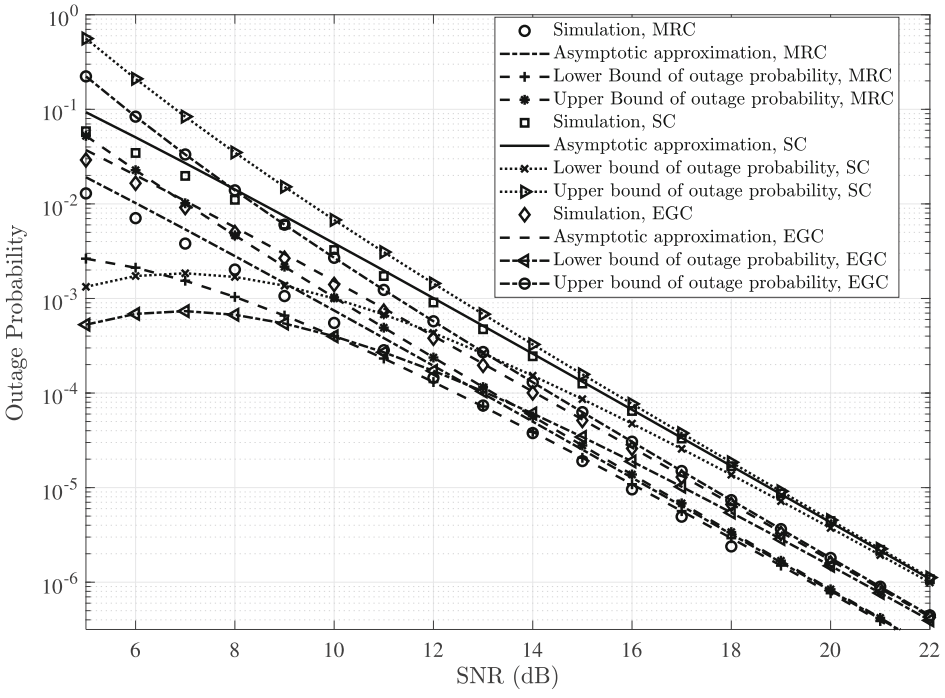

Fig. 1 OP curves for the asymptotic approximation, lower bound, and upper bound for MRC, SC, and EGC over correlated BX fading channels. The number of branches is $N = 2$, the fading parameter is $m = 1.5$, and the correlation structure is $\mathbf{C_b} = \left[\mathbf{C}_1, \mathbf{0}_{2\times2}, \mathbf{0}_{2\times2}; \mathbf{0}_{2\times2}, \mathbf{C}_2, \mathbf{0}_{2\times2}; \mathbf{0}_{2\times2}, \mathbf{0}_{2\times2}, \mathbf{C}_3\right]$, where $\mathbf{C}_1 = \mathbf{C}_2 = \mathbf{C}_3 = \left[1, \sqrt{0.35}; \sqrt{0.35}, 1\right]$

$$V(R_{\text{th}}) = \int_{R_{\text{SC}}>R_{\text{th}}^2} Q\left(\sqrt{q \max_n \left\{\sum_{i=1}^{2m} b_{n,i}^2\right\}}\right) d\mathbf{b} = \left\{\frac{\pi^{\text{mN}} 2^{\text{mN}-1}}{q^{\text{mN}}\sqrt{\pi}} \frac{\Gamma\left(\text{mN}+\frac{1}{2}\right)}{\Gamma^N(m+1)}\right.$$
$$\left. - \frac{\pi^{\text{mN}}}{\Gamma^N(m+1)}\left[R_{th}^{2\text{mN}} Q\left(\sqrt{q}R_{\text{th}}\right) + \frac{2^{\text{mN}-1}}{q^{\text{mN}}\sqrt{\pi}}\gamma\left(\text{mN}+\frac{1}{2}, \frac{q}{2}R_{\text{th}}^2\right)\right]\right\}. \quad (81)$$

The upper error rate bound for SC is obtained by substituting (78) and (81) into (80).

9 Discussion on the tightness of the bounds

9.1 Tightness of the outage probability bound

We consider the exponential component of the lower bounds of the OP for MRC, EGC, and SC, in (26), (36), and (44), respectively, and also that of the upper bound shown in (28), (38), and (46), respectively. Comparing the asymptotic approximations, the lower and the upper bounds of each of the diversity combining schemes, it is seen that the difference lies in the exponential components of each of the expressions. We note that an increase to the average SNR per branch by a factor P results in an increase in the covariance matrix $\mathbf{R_b}$ and eventually a decrease in $\mathbf{R_b^{-1}}$ by the same factor. This leads to a decrease in the value of $\lambda_{\max}$ (which is the largest eigenvalue of $\mathbf{R_b^{-1}}$) by that same factor, i.e., $\frac{\lambda_{\max}}{P}$. With this in mind, we can express the limit of the ratio of lower bound OP to the upper bound OP as P tends to infinity as

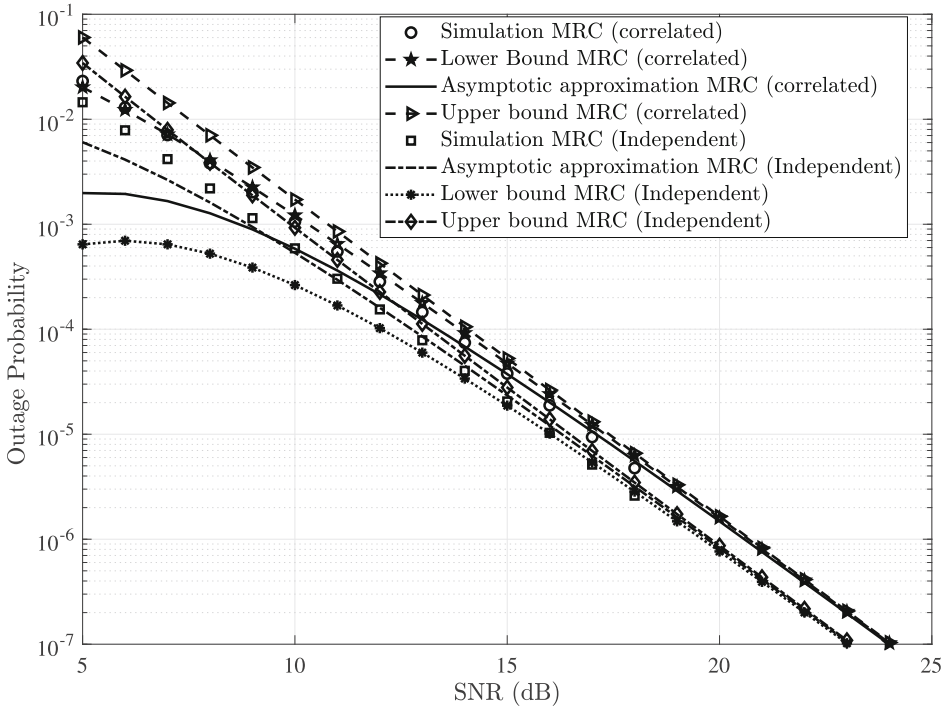

Fig. 2 OP curves for the asymptotic approximation, lower bound, and upper bound for MRC over correlated and independent BX fading channels. The number of branches is $N = 2$, the fading parameter is $m = 1.5$, and the correlation structure is $\mathbf{C_b} = \left[\mathbf{C}_1, \mathbf{0}_{2\times2}, \mathbf{0}_{2\times2}; \mathbf{0}_{2\times2}, \mathbf{C}_2, \mathbf{0}_{2\times2}; \mathbf{0}_{2\times2}, \mathbf{0}_{2\times2}, \mathbf{C}_3\right]$, where $\mathbf{C}_1 = \mathbf{C}_2 = \mathbf{C}_3 = \left[1, \sqrt{0.35}; \sqrt{0.35}, 1\right]$ and $\mathbf{C}_1 = \mathbf{C}_2 = \mathbf{C}_3 = [1, 0; 0, 1]$ are for correlation and independence, respectively

$$\lim_{P\to\infty}\frac{P_{o,\mathrm{LB}}\left(\gamma_{\mathrm{th}}\right)}{P_{o,\mathrm{UB}}\left(\gamma_{\mathrm{th}}\right)}=\frac{\exp\left(-\frac{1}{2}\left(\frac{\lambda_{\max}\gamma_{\mathrm{th}}}{P}+2\left\|\frac{\boldsymbol{\mu}_{\mathbf{b}}^{T}\mathbf{R}_{\mathbf{b}}^{-1}}{P}\right\|\sqrt{\gamma_{\mathrm{th}}}\right)\right)}{\exp\left(\left\|\frac{\boldsymbol{\mu}_{\mathbf{b}}^{T}\mathbf{R}_{\mathbf{b}}^{-1}}{P}\right\|\sqrt{\gamma_{\mathrm{th}}}\right)}. \tag{82}$$

Equation 82 shows that the lower and upper bounds of the OP converge to the asymptotic approximation as the SNR approaches infinity. This property is highly desirable.

9.2 Tightness of the error rate bound

Given the definition of the incomplete gamma function

$$\Gamma\left(s\right)=\lim_{x\to\infty}\gamma\left(s,x\right) \tag{83}$$

and the Chernoff bound of the Q-function [20, 27]

$$Q\left(x\right)\leq e^{-\frac{x^{2}}{2}},\quad x>0 \tag{84}$$

we apply these definitions to $G(R_{\mathrm{th}})$, $H(R_{\mathrm{th}})$, $W(R_{\mathrm{th}})$, $Z(R_{\mathrm{th}})$, $S(R_{\mathrm{th}})$, and $V(R_{\mathrm{th}})$ in (54), (49), (65), (71), (78), and (81), respectively, to show the tightness of the bit-error rate (BER) bounds, according to

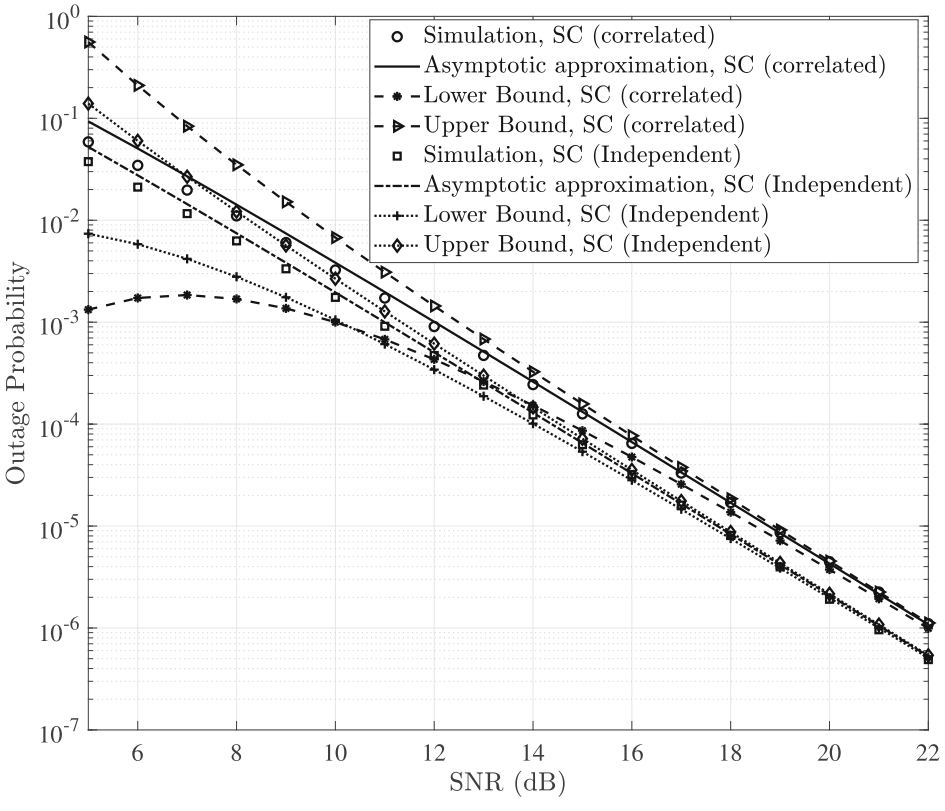

Fig. 3 OP curves for the asymptotic approximation, lower bound, and upper bound for SC over correlated and independent BX fading channels. The number of branches is $N=2$, the fading parameter is $m=1.5$, and the correlation structure is $\mathbf{C_b}=\left[\mathbf{C}_1,\mathbf{0}_{2\times2},\mathbf{0}_{2\times2};\mathbf{0}_{2\times2},\mathbf{C}_2,\mathbf{0}_{2\times2};\mathbf{0}_{2\times2},\mathbf{0}_{2\times2},\mathbf{C}_3\right]$, where $\mathbf{C}_1=\mathbf{C}_2=\mathbf{C}_3=\left[1,\sqrt{0.35};\sqrt{0.35},1\right]$ and $\mathbf{C}_1=\mathbf{C}_2=\mathbf{C}_3=[1,0;0,1]$ are for the correlated and independent cases, respectively

$$\lim_{R_{\text{th}}\to\infty} G(R_{\text{th}}) = \frac{2^{\text{mN}-1}\pi^{\text{mN}}}{q^{\text{mN}}\sqrt{\pi}} \frac{\Gamma\left(\text{mN}+\frac{1}{2}\right)}{\Gamma\left(\text{mN}+1\right)} \tag{85}$$

$$\lim_{R_{\text{th}}\to\infty} H(R_{\text{th}}) = 0 \tag{86}$$

$$\lim_{R_{\text{th}}\to\infty} W(R_{\text{th}}) = Y(R_{\text{th}}) \tag{87}$$

$$\lim_{R_{\text{th}}\to\infty} Z(R_{\text{th}}) = Y(R_{\text{th}}) - \frac{\pi^{\text{mN}-\frac{1}{2}}}{\Gamma\left(\text{mN}+1\right)} \times \left[\frac{2^{\text{mN}-1}}{q^{\text{mN}}}\Gamma\left(\text{mN}+\frac{1}{2}\right)\right] \tag{88}$$

$$\lim_{R_{\text{th}}\to\infty} S(R_{\text{th}}) = \frac{2^{\text{mN}-1}\pi^{\text{mN}}}{q^{\text{mN}}\sqrt{\pi}} \frac{\Gamma\left(\text{mN}+\frac{1}{2}\right)}{\Gamma^{N}\left(m+1\right)} \tag{89}$$

$$\lim_{R_{\text{th}}\to\infty} V(R_{\text{th}}) = 0. \tag{90}$$

We then consider the exponential component, where we see that an increase in the average SNR per branch by a factor P results in an increase in the covariance matrix $\mathbf{R_b}$.

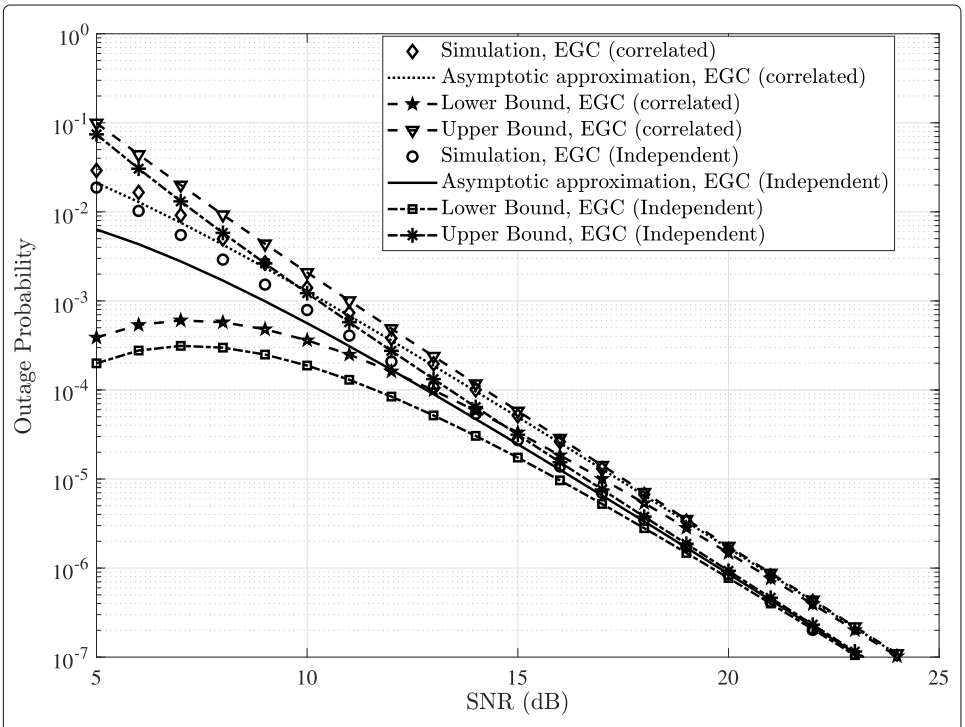

Fig. 4 OP curves for the asymptotic approximation, lower bound, and upper bound for EGC over correlated and independent BX fading channels. The number of branches is $N = 2$, the fading parameter is $m = 1.5$, and the correlation structure is $\mathbf{C_b} = \left[\mathbf{C}_1, \mathbf{0}_{2\times2}, \mathbf{0}_{2\times2}; \mathbf{0}_{2\times2}, \mathbf{C}_2, \mathbf{0}_{2\times2}; \mathbf{0}_{2\times2}, \mathbf{0}_{2\times2}, \mathbf{C}_3\right]$, where $\mathbf{C}_1 = \mathbf{C}_2 = \mathbf{C}_3 = \left[1, \sqrt{0.8}; \sqrt{0.8}, 1\right]$ and $\mathbf{C}_1 = \mathbf{C}_2 = \mathbf{C}_3 = [1, 0; 0, 1]$ are for correlated and independent cases, respectively

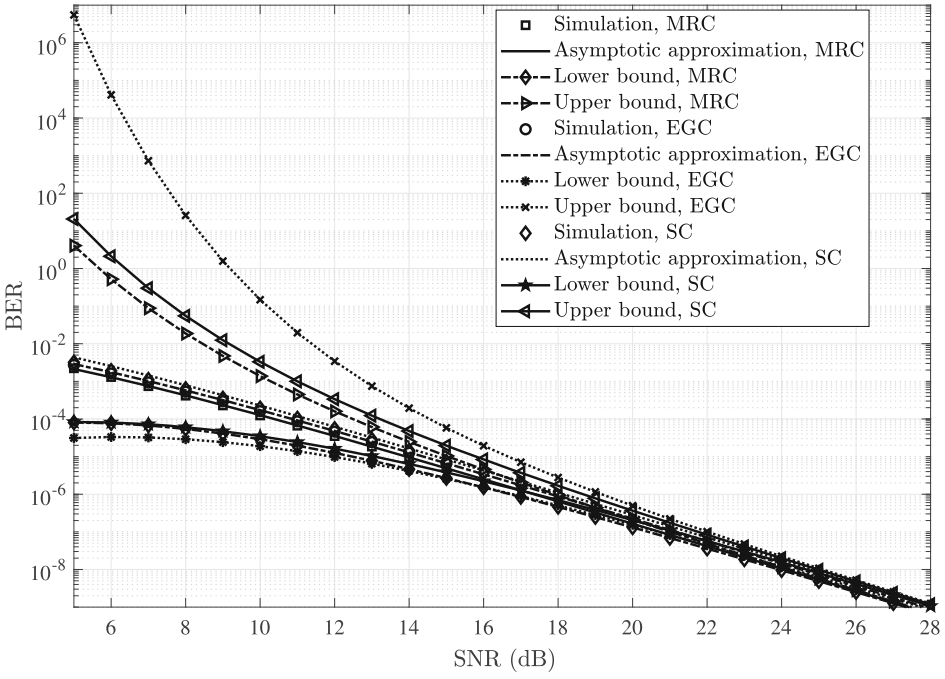

Fig. 5 BER curves for the asymptotic approximation, lower bound, and upper bound for MRC, SC, and EGC, over correlated BX fading channels. The number of branches is $N = 2$, the fading parameter is $m = 1.5$, and the correlation structure is $\mathbf{C_b} = \left[\mathbf{C}_1, \mathbf{0}_{2\times2}, \mathbf{0}_{2\times2}; \mathbf{0}_{2\times2}, \mathbf{C}_2, \mathbf{0}_{2\times2}; \mathbf{0}_{2\times2}, \mathbf{0}_{2\times2}, \mathbf{C}_3\right]$, where $\mathbf{C}_1 = \mathbf{C}_2 = \mathbf{C}_3 = \left[1, \sqrt{0.4}; \sqrt{0.4}, 1\right]$

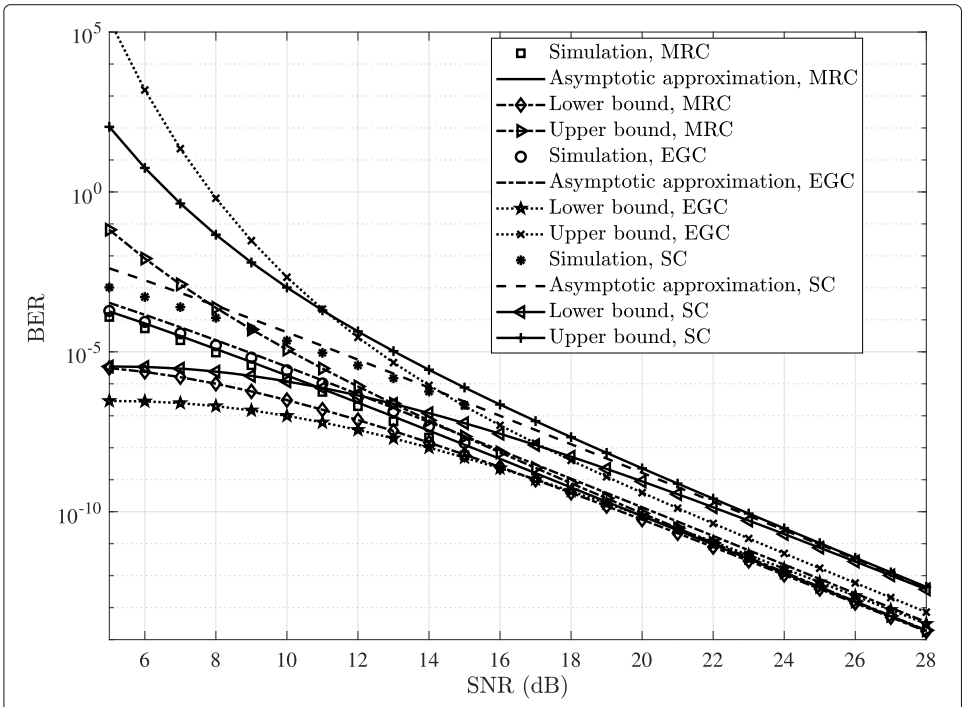

Fig. 6 BER curves for the asymptotic approximation, lower bound, and upper bound for MRC, SC, and EGC, over correlated BX fading channels. The number of branches is $N = 3$, the fading parameter is $m = 1.5$, and the correlation structure is $\mathbf{C_b} = \left[\mathbf{C}_1, \mathbf{0}_{3\times3}, \mathbf{0}_{3\times3}; \mathbf{0}_{3\times3}, \mathbf{C}_2, \mathbf{0}_{3\times3}; \mathbf{0}_{3\times3}, \mathbf{0}_{3\times3}, \mathbf{C}_3\right]$, where $\mathbf{C}_1 = \mathbf{C}_2 = \mathbf{C}_3 = \left[1, \sqrt{0.4}, \sqrt{0.2}; \sqrt{0.4}, 1, \sqrt{0.4}; \sqrt{0.2}, \sqrt{0.4}, 1\right]$

This leads to a decrease in $\mathbf{R}_{\mathbf{b}}^{-1}$ and eventually a decrease in $\lambda_{\max}$ by the same factor P. Thus, we find the limit to be

$$\lim_{P\to\infty}\frac{P_{e,\mathrm{LB}}}{P_{e,\mathrm{UB}}}=\frac{\exp\left(-\frac{1}{2}\left(\frac{\lambda_{\max}R_{\mathrm{th}}^2}{P}+2\left\|\frac{\boldsymbol{\mu}_{\mathbf{b}}^T\mathbf{R}_{\mathbf{b}}^{-1}}{P}\right\|R_{\mathrm{th}}\right)\right)}{\exp\left(\left\|\frac{\boldsymbol{\mu}_{\mathbf{b}}^T\mathbf{R}_{\mathbf{b}}^{-1}}{P}\right\|R_{\mathrm{th}}\right)}. \tag{91}$$

Expressing R_{th} in terms of P, i.e., $R_{\mathrm{th}}=\sqrt{P}$, gives

$$\lim_{P\to\infty}\frac{P_{e,\mathrm{LB}}}{P_{e,\mathrm{UB}}}=\frac{\exp\left(-\frac{1}{2}\left(\frac{\lambda_{\max}R_{\mathrm{th}}^2}{P}+2\left\|\frac{\boldsymbol{\mu}_{\mathbf{b}}^T\mathbf{R}_{\mathbf{b}}^{-1}}{P}\right\|\sqrt{P}\right)\right)}{\exp\left(\left\|\frac{\boldsymbol{\mu}_{\mathbf{b}}^T\mathbf{R}_{\mathbf{b}}^{-1}}{P}\right\|\sqrt{P}\right)}. \tag{92}$$

This property is highly desirable.

10 Numerical results

Figure 1 shows a comparison of OP curves for MRC, SC, and EGC for a 2-branch diversity system over correlated BX fading channels with coherent BPSK modulation and a fading parameter of $m=1.5$. Correlation structure of the form $\mathbf{C_b}=[\mathbf{C}_1,\mathbf{0}_{2\times2},\mathbf{0}_{2\times2};\mathbf{0}_{2\times2},\mathbf{C}_2;\mathbf{0}_{2\times2},\mathbf{0}_{2\times2},\mathbf{0}_{2\times2},\mathbf{C}_3]$, where $\mathbf{C}_1=\mathbf{C}_2=\mathbf{C}_3=\left[1,\sqrt{0.35};\sqrt{0.35},1\right]$, is considered. The lower and upper bounds converge to the asymptotic approximation and simulated OPs at high SNR. It is observed that the OPs of MRC and EGC are close to each other unlike

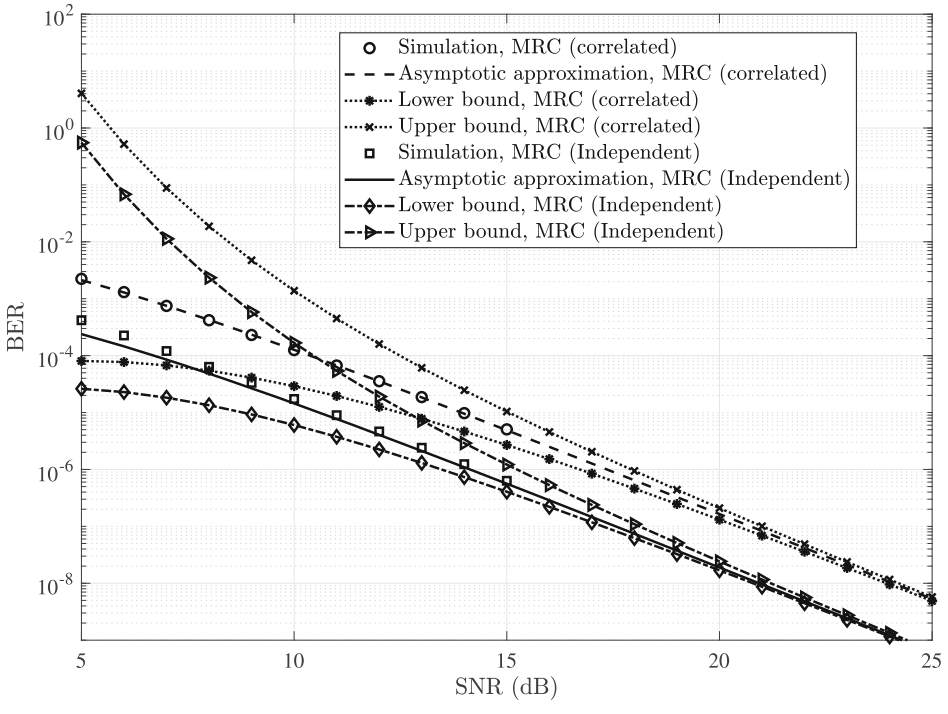

Fig. 7 BER curves for the asymptotic approximation, lower bound, and upper bound for MRC, over correlated and independent BX fading channels. The number of branches is $N=2$, the fading parameter is $m=1.5$, and the correlation structures is $\mathbf{C_b}=\left[\mathbf{C}_1,\mathbf{0}_{2\times2},\mathbf{0}_{2\times2};\mathbf{0}_{2\times2},\mathbf{C}_2,\mathbf{0}_{2\times2};\mathbf{0}_{2\times2},\mathbf{0}_{2\times2},\mathbf{C}_3\right]$, where $\mathbf{C}_1=\mathbf{C}_2=\mathbf{C}_3=\left[1,\sqrt{0.4};\sqrt{0.4},1\right]$ and $\mathbf{C}_1=\mathbf{C}_2=\mathbf{C}_3=[1,0;0,1]$ are for correlated and independent cases, respectively

MRC and SC. This is largely due to the factor contributed by the integral in (23), (31), and (41).

Figures 2, 3, and 4 show a comparison of OP curves of MRC, SC, and EGC, respectively, for a 2-branch diversity system over correlated and independent BX fading channels with coherent BPSK modulation and a fading parameter of $m = 1.5$. Correlation structure of the form $\mathbf{C_b} = [\mathbf{C}_1, \mathbf{0}_{2\times2}, \mathbf{0}_{2\times2}; \mathbf{0}_{2\times2}, \mathbf{C}_2, \mathbf{0}_{2\times2}; \mathbf{0}_{2\times2}, \mathbf{0}_{2\times2}, \mathbf{C}_3]$, where $\mathbf{C}_1 = \mathbf{C}_2 = \mathbf{C}_3 = \begin{bmatrix} 1, \sqrt{0.35}; & \sqrt{0.35}, 1 \end{bmatrix}$ and $\mathbf{C}_1 = \mathbf{C}_2 = \mathbf{C}_3 = [1, 0; 0, 1]$, is considered for correlation and independence, respectively. The independent channels outperform the correlated channels, as expected. The effect of correlation is seen on the rate of convergence exhibited by the three combining techniques.

Figure 5 shows a comparison of BER curves for MRC, SC, and EGC for a 2-branch diversity system over correlated BX fading channels with coherent BPSK modulation and a fading parameter of $m = 1.5$ with a correlation matrix of the form $\mathbf{C_b} = [\mathbf{C}_1, \mathbf{0}_{2\times2}, \mathbf{0}_{2\times2}; \mathbf{0}_{2\times2}, \mathbf{C}_2, \mathbf{0}_{2\times2}; \mathbf{0}_{2\times2}, \mathbf{0}_{2\times2}, \mathbf{C}_3]$, where $\mathbf{C}_1 = \mathbf{C}_2 = \mathbf{C}_3 = \begin{bmatrix} 1, \sqrt{0.4}; \sqrt{0.4}, 1 \end{bmatrix}$. The lower and upper bounds again converge to the asymptotic approximation at high SNR. It is seen that the BERs for MRC and EGC are close to each other, differing by at most 3 dB.

Figure 6 shows a comparison of BER curves for MRC, SC, and EGC for a 3-branch diversity system over correlated BX fading channels with coherent BPSK modulation and a fading parameter of $m = 1.5$ with a correlation matrix of the form $\mathbf{C_b} = [\mathbf{C}_1, \mathbf{0}_{3\times3}, \mathbf{0}_{3\times3}; \mathbf{0}_{3\times3}, \mathbf{C}_2, \mathbf{0}_{3\times3}; \mathbf{0}_{3\times3}, \mathbf{0}_{3\times3}, \mathbf{C}_3]$, where $\mathbf{C}_1 = \mathbf{C}_2 = \mathbf{C}_3 = \begin{bmatrix} 1, \sqrt{0.4}, \sqrt{0.2}; \sqrt{0.4}, 1, \sqrt{0.4}; \sqrt{0.2}, \sqrt{0.4}, 1 \end{bmatrix}$. The bounds are seen to be tight at high SNR.

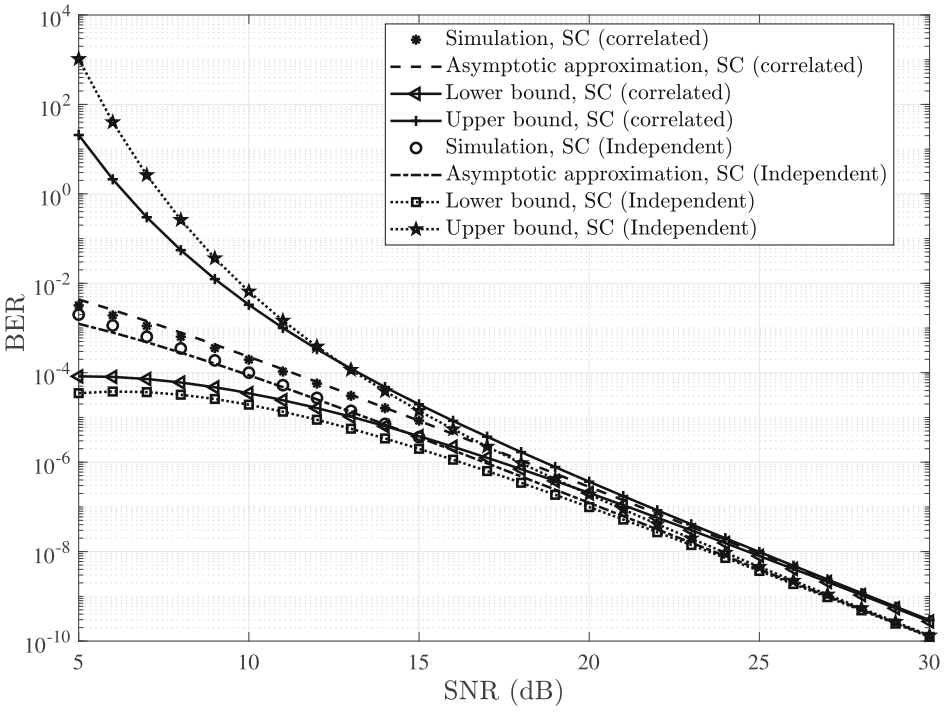

Fig. 8 BER curves for the asymptotic approximation, lower bound, and upper bound for SC, over correlated and independent BX fading channels. The number of branches is $N = 2$, the fading parameter is $m = 1.5$, and the correlation structures is $\mathbf{C_b} = \begin{bmatrix} \mathbf{C}_1, \mathbf{0}_{2\times2}, \mathbf{0}_{2\times2}; \mathbf{0}_{2\times2}, \mathbf{C}_2, \mathbf{0}_{2\times2}; \mathbf{0}_{2\times2}, \mathbf{0}_{2\times2}, \mathbf{C}_3 \end{bmatrix}$, where $\mathbf{C}_1 = \mathbf{C}_2 = \mathbf{C}_3 = \begin{bmatrix} 1, \sqrt{0.4}; \sqrt{0.4}, 1 \end{bmatrix}$ and $\mathbf{C}_1 = \mathbf{C}_2 = \mathbf{C}_3 = [1, 0; 0, 1]$ are for correlated and independent cases, respectively

It is observed that the BERs for MRC and EGC are again close to each other, differing by at most 3 dB in SNR.

Figures 7, 8, and 9 show a comparison of BER curves for MRC, SC, and EGC, for a 2-branch diversity system over correlated and independent BX fading channels with coherent BPSK modulation and a fading parameter of $m = 1.5$ with a correlation matrix of the form $\mathbf{C_b} = [\mathbf{C}_1, \mathbf{0}_{2\times2}, \mathbf{0}_{2\times2}; \mathbf{0}_{2\times2}, \mathbf{C}_2, \mathbf{0}_{2\times2};\ \mathbf{0}_{2\times2}, \mathbf{0}_{2\times2}, \mathbf{C}_3]$, where $[\mathbf{C}_1 = \mathbf{C}_2 = \mathbf{C}_3 = \left[1, \sqrt{0.4};\ \sqrt{0.4}, 1\right]$ and $\mathbf{C}_1 = \mathbf{C}_2 = \mathbf{C}_3 = [1, 0; 0, 1]$ for correlated and independent cases. The performance improves when the channels are independent. The effect of the correlation matrix is also seen in the rate of convergence of the bounds, i.e., the higher the determinant of $\mathbf{C_b}$ (signifying greater independence between channels), the faster the rate of convergence.

Our general results can be formulated into the special case of the Nakagami-m fading model, with $\mu = 0$, the results of which are shown in [17]. The relationship between the power correlation coefficients and associated Gaussian correlation coefficients when $\mu = 0$ is obtained in Section 3. We also compare the bound on the pdf of the channel coefficient obtained in (20) when $\mu = 0$ to the result obtained in [17], such that (20) becomes

$$f_{\mathbf{b}}(\mathbf{0}) \exp\left(-\frac{1}{2}\lambda_{\max} r\right) \leq f_{\mathbf{b}}(\mathbf{b}) \leq f_{\mathbf{b}}(\mathbf{0}). \tag{93}$$

This leads to the following insights.

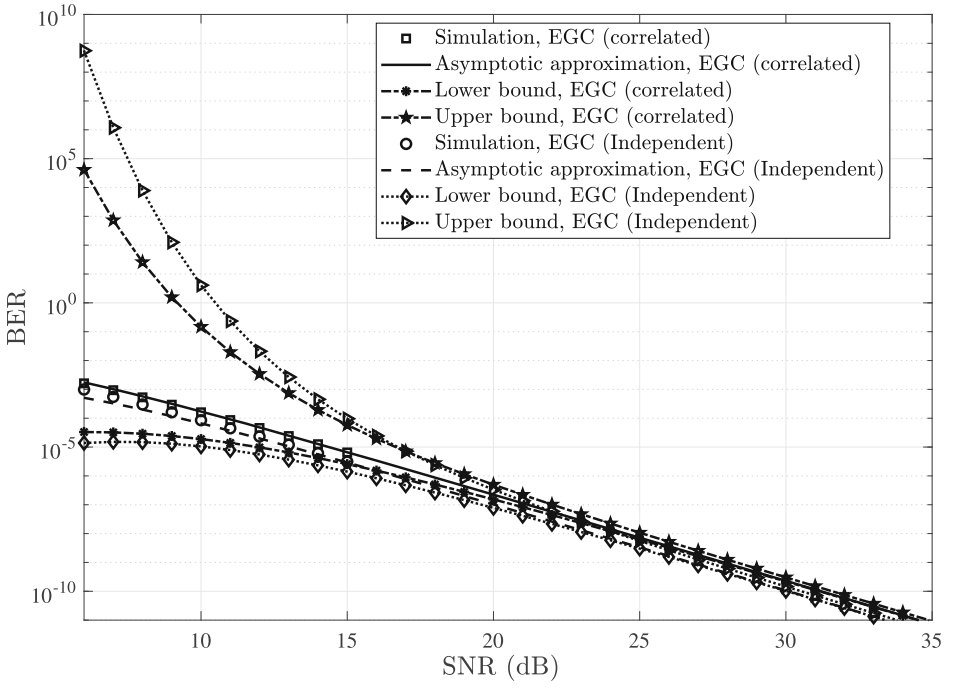

Fig. 9 BER curves for the asymptotic approximation, lower bound, and upper bound for EGC, over correlated and independent BX fading channels. The number of branches is $N = 2$, the fading parameter is $m = 1.5$, and the correlation structures is $\mathbf{C_b} = \left[\mathbf{C}_1, \mathbf{0}_{2\times2}, \mathbf{0}_{2\times2}; \mathbf{0}_{2\times2}, \mathbf{C}_2, \mathbf{0}_{2\times2}; \mathbf{0}_{2\times2}, \mathbf{0}_{2\times2}, \mathbf{C}_3\right]$, where $\mathbf{C}_1 = \mathbf{C}_2 = \mathbf{C}_3 = \left[1, \sqrt{0.4}; \sqrt{0.4}, 1\right]$ and $\mathbf{C}_1 = \mathbf{C}_2 = \mathbf{C}_3 = [1, 0; 0, 1]$ are for correlated and independent cases, respectively

- The asymptotic approximation and the upper bound of the outage probabilities and error rates are the same for the combining schemes under consideration, which agree with the conclusions in [17].
- The results here differ from the results in [17] in that this analysis for the new fading channel include multiple LOS and non-LOS components and can be suitable for environments without LOS components when $\mu = 0$.
- The expressions for the pdf bounds in (83) are the same as the pdf bound obtained in [17].
- Our results bring about meaningful comparison between the BX and abovementioned fading models.

11 Conclusion

In this work, we derived asymptotically tight lower and upper bounds for the OP and BER of correlated BX fading channels. The effects of certain channel characteristics (e.g., presence of LOS components, diversity combining techniques, and channel correlation) were observed on the performance of the communication system. The special case of our results in the absence of LOS components agrees with those obtained for the Nakagami-m fading model in [17], which confirms the accuracy and reproducibility of our work. Ultimately, our results show the accuracy of the BX fading model in characterizing wireless communication environments with both LOS and non-LOS components.

Abbreviations

BER: Bit-error rate; BPSK: Binary phase shift keying; EGC: Equal-gain combining; LOS: Line-of-sight; LB: Lower bound; LE: Lower bound of EGC; LS: Lower bound of SC; LM: Lower bound of MRC; MRC: Maximal ratio combining; OP: Outage probability; RV: Random variable; SC: Selection combining; UB: Upper bound; UE: Upper bound of EGC; US: Upper bound of SC; UM: Upper bound of MRC

Acknowledgements

We thank Dr. Norman Beaulieu for his careful proof-reading of an earlier version of the paper.

Authors' contributions

AO derived the equations and performed the system simulations. JC and JFH revised the equations and contributed to the writing of the manuscript. JC proposed the main idea and the authors read and approved the final manuscript.

Funding

This work was supported by the Natural Sciences Engineering Research Council of Canada.

Availability of data and materials

The paper is self-contained as we provided all mathematical derivations and framework in Sections 3–7. We have also described in details numerical results and parameter settings (values) in Section 8 for ease of result reproduction.

Competing interests

The authors declare that they have no competing interests.

Received: 18 November 2018 Accepted: 13 April 2020
Published online: 13 May 2020

References

1. N. C. Beaulieu, J. Xie, A novel fading model for channels with multiple dominant specular components. IEEE Wirel. Commun. Lett. **4**(1), 54–57 (2015)
2. M. D. Yacoub, Nakagami-m phase-envelope joint distribution: a new model. IEEE Trans. Veh. Technol. **59**(3), 1552–1557 (2010)
3. N. C. Beaulieu, S. A. Saberali, in *Proc. IEEE ICC 2014*, A generalized diffuse scatter plus line-of-sight fading channel model (IEEE, Sydney, 2014), pp. 5849–5853
4. S. Wyne, A. P. Singh, F. Tufvesson, A. F. Molisch, A statistical model for indoor office wireless sensor channels. IEEE Trans. Wirel. Commun. **8**(8), 4154–4164 (2009)
5. M. K. Samimi, G. R. MacCartney, S. Sun, T. S. Rappaport, in *Proc. IEEE 83rd Veh. Technol. Conf. (VTC Spring)*, 28 GHz millimeter-wave ultrawideband small-scale fading models in wireless channels (IEEE, Nanjing, 2016), pp. 1–6
6. A. Olutayo, J. Cheng, J. F. Holzman, in *Proc. IEEE ICC 2017*, Asymptotically tight performance bounds for selection combining over new fading channels with arbitrary correlation (IEEE, Paris, 2017)

7. A. Olutayo, H. Ma, J. Cheng, J. F. Holzman, Level crossing rate and average fade duration for a new fading model. IEEE Wirel. Commun. Lett. **6**(3), 326–329 (2017)
8. J. Hu, Z. Zhang, J. Dang, L. Wu, G. Zhu, Performance of decode-and-forward relaying in mixed Beaulieu-Xie and M dual-Hop transmission systems with digital coherent detection. IEEE Open Access. **7**, 138757–138770 (2019)
9. L. Zhang, C. Liu, J. Zhang, F. Wu, W. Yang, Performance of relay networks in fading environments with dominant specular components. China Commun. **13**(12), 69–78 (2016)
10. P.S. Chauchan, S. Kumar, S.K. Soni, On the physical layer security over Beaulieu-Xie fading channel. AEU Int. J. Electr. Commun. **113**(152940) (2020)
11. B. Zhu, Z. Zeng, J. Cheng, N. C. Beaulieu, On the distribution function of the generalized Beckmann random variable and its applications in communications. IEEE Trans. Commun. **66**(6), 2235–2250 (2018)
12. X. Wang, N. C. Beaulieu, Switching rates of two-branch selection diversity in κ-μ and α-mu distributed fadings. IEEE Trans. Wirel. Commun. **8**(4), 1667–1671 (2009)
13. M. R. Bhatnagar, On the sum of correlated κ-mu shadowed random variables and its application to performance analysis of MRC. IEEE Trans. Veh. Technol. **64**(6), 2678–2684 (2015)
14. M. Schwartz, W. R. Bennett, S. Stein, *Communication systems and techniques*. (IEEE Press, New York, 1996)
15. V. A. Aalo, Performance of maximal-ratio diversity systems in a correlated Nakagami-fading environment. IEEE Trans. Commun. **43**(8), 2360–2369 (1995)
16. V. V. Veeravalli, On performance analysis for signaling on correlated fading channels. IEEE Trans. Commun. **49**(11), 1879–1883 (2001)
17. B. Zhu, F. Yang, J. Cheng, L. Wu, Performance bounds for diversity receptions over arbitrarily correlated Nakagami-m fading channel. IEEE Trans. Wirel. Commun. **15**(1), 699–713 (2016)
18. A. Papoulis, *Probability, random variables, and stochastic processes, 3rd ed*. (McGraw-Hill, New York, 1991)
19. R. A. Horn, C. R. Johnson, *Matrix Analysis*. (Cambridge Univ. Press, Cambridge, 2013)
20. M. Chiani, D. Dardari, M. K. Simon, New exponential bounds and approximations for the computation of error probability in fading channels. IEEE Trans. Wirel. Commun. **2**(4), 840–845 (2003)
21. E. W. Ng, M. Geller, A table of integrals of the error function. J. Res. Natl. Bur. Stand. B. **73**(1), 1–20 (1969)
22. S. Liu, J. Cheng, N. C. Beaulieu, Asymptotic error analysis of diversity schemes on arbitrarily correlated Rayleigh channel. IEEE Trans. Commun. **58**(5), 1351–1355 (2010)
23. X. Li, J. Cheng, Asymptotic error rates analysis of selection combining on generalised correlated Nakagami-m channels. IEEE Trans. Commun. **60**(7), 1765–1771 (2012)
24. M. Z. Win, G. Chrisikos, J. H. Winters, MRC performance for *M*-ary modulation in arbitrarily correlated Nakagami fading channels. IEEE Commun. Lett. **4**(10), 301–303 (2000)
25. Q. T. Zhang, Maximal-ratio combining over Nakagami fading channels with an arbitrary branch covariance matrix. IEEE Trans. Veh. Technol. **48**(4), 1141–1150 (1999)
26. P. Lombardo, G. Fedele, M. M. Rao, MRC performance for binary signals in Nakagami fading with general branch correlation. IEEE Trans. Commun. **47**(1), 44–52 (1999)
27. I. S. Gradshteyn, I. M. Ryzhik, *Table of Integrals, Series, and Products, 6th ed*. (Academic, New York, 2000)

Publisher's Note